

The Stochastic Ferrous Wheel and its Implications for the Carbon Cycle

Aidan J. Matthews

Advised by Amilcare Porporato

April 2024

Submitted in partial fulfillment of the requirements for the degree of
Bachelor of Science in Engineering Department of Civil and
Environmental Engineering Princeton University.

I hereby declare that I am the sole author of this thesis.

I authorize Princeton University to lend this thesis to other institutions or individuals for the purpose of scholarly research.

A handwritten signature in cursive script that reads "Aidan Matthews". The signature is written in black ink and has a fluid, connected style.

Aidan J. Matthews

I further authorize Princeton University to reproduce this thesis by photocopying or by other means, in total or in part, at the request of other institutions or individuals for the purpose of scholarly research.

A handwritten signature in cursive script that reads "Aidan Matthews". The signature is written in black ink and has a fluid, connected style.

Aidan J. Matthews

Abstract

The soil iron cycle has a multi-faceted role in the soil carbon cycle affecting carbon emissions across the globe. The drivers of the iron cycle or “ferrous wheel” are fluctuating redox conditions caused by changes in soil moisture. Soil moisture may change due to stochastic inputs (rainfall) or deterministic events (irrigation) over hours or over months. Various aspects of the soil iron cycle have been studied from a microbiological or geochemical perspective, but modeling the macroscopic effects of the cycle remains a challenge [22, 36, 118]. Two of the most critical mechanisms in which iron affects soil carbon storage are (I) the protection of carbon by iron oxides and (II) the oxidation of carbon with iron as an electron acceptor. These two effects have not yet been explicitly modeled together. Furthermore, many studies are limited to the effect of constant length redox cycles, and the effect of stochastic fluctuations of soil moisture has not been thoroughly explored [21, 22, 124]. The objective of this thesis is to investigate how the coupled water-iron-carbon cycles behave under different conditions and how these interactions affect carbon emissions. To tackle this open ended question, this thesis develops a first pass model at capturing these dynamics. The model is divided into two components: (I) a numerical model that includes carbon protection and carbon oxidation by iron reduction, and (II) a simplified model of the iron cycle driven by stochastic soil moisture fluctuations. Through simulations, the numerical model demonstrates that different initial conditions and rates of reduction can alter the net effect (positive or negative) of iron on carbon emissions. From the stochastic model a probability density function was derived of the fraction of iron that is reduced in a fluctuating redox environment. This function has broad applicability to both carbon dynamics and iron properties of the soil. Overall the models progress the current state of modeling the iron and carbon cycles and connect existing conceptions to a mathematical modeling framework, an important step for predicting soil carbon dynamics under climate change.

Acknowledgements

I'd like to thank my advisor Amilcare Porporato without whom nothing written below would have been possible – in many senses. This thesis also stands on the shoulders of Salvatore Calabrese who wrote the papers this work is based on. I would also like to thank the entire Princeton CEE department for inspiring me to pursue environmental engineering through their teaching, including Professors Michael Celia, Elie Bou-Zeid, Reed Maxwell, Peter Jaffe, and Branko Glisic.

I thank my friends at Princeton, and especially Sarah Pedersen for her invaluable lessons on where, and where, not to place, commas. I'd like to thank my parents, my parents' parents, my parents' parents' parents, and all sixteen of my parents' parents' parents' parents' for always believing in me. I'd also like to thank the entire faculty and staff at SCHouse for their emotional and academic support.

Contents

Abstract	2
Acknowledgements	3
1 Introduction	6
1.1 Motivation	6
1.2 Approach	7
1.3 The Challenges of Environmental Models	9
2 Literature Review	10
2.1 The soil carbon cycle	10
2.1.1 Redox Potential and Decomposition	11
2.1.2 Carbon Stabilization	12
2.1.3 Mineral Association	13
2.2 The Iron Cycle	15
2.2.1 Iron Reduction in Soil	16
2.2.2 Iron Oxidation	18
2.3 The Coupled Water-Iron-Carbon Cycles	18
2.4 Modeling Soil Processes	20
2.4.1 Compartment Models	20
2.4.2 Soil Moisture Models	21
2.4.3 Iron Cycle Models	22
2.4.4 Carbon Cycle	24
2.4.5 Modeling the Coupled Water-Iron-Carbon Cycle	26
2.5 Stochasticity in Environmental Models	27
2.6 Summary	29
3 A Numerical Model of the Water-Iron-Carbon Cycles	31
3.1 Bucket Soil Moisture Model	31
3.1.1 Rainfall Modelling	32
3.2 Iron Cycle	33
3.3 Carbon Cycle	35
3.3.1 Mineral Association	36
3.4 Steady State Analysis	37
3.5 Model Set Up	39
3.5.1 Parameterization	40
3.5.2 Simulations	42

3.6	Results	43
3.6.1	Results: Static Soil Moisture	44
3.6.2	Results: Redox Cycles	46
3.6.3	Results: Stochastic Soil Moisture	46
3.7	Discussion	48
4	Analytical Solution to the Stochastic Ferrous Wheel	52
4.1	Problem Formulation	52
4.2	Deriving the Steady State Probability Density Function	55
4.2.1	Mean	59
4.2.2	Crossing Times	59
4.3	A simplified Soil Moisture Model	61
4.4	Quantifying Total Reduction	64
4.5	Average Protection Capacity	69
4.6	Results and Discussion	69
4.6.1	Overview	69
4.6.2	Implications	71
5	Conclusion	76
5.1	Key Points	76
5.2	Summary	77
5.3	Limitations and Future Work	79
6	Appendix	81
6.1	Appendix A: Assumption of a Constant Reactive Iron Pool.	81
6.2	Appendix B: Assumption of Exponential Crossing Times	82

Chapter 1

Introduction

1.1 Motivation

Together, iron and carbon make steel, a substance that is stronger than the sum of its parts, a non-linear interaction. In soil, iron and carbon also interact in non-linear ways, affecting the decomposition of carbon into the critical greenhouse gases carbon dioxide and methane [36, 64, 77, 125, 139, 141]. The soil iron cycle or “ferrous wheel” (term first coined by Glusker 1968 in a different context [47]) is driven by redox conditions which are determined by hydrologic forcings (precipitation, irrigation, or flooding) [22, 88, 97, 124, 134, 145]. The soil, critical to humanity as a major store of organic carbon in the form of soil organic matter (SOM), encompasses an estimated 1400 to 2400 Gt of carbon stored in the soil, with an additional 1700 Gt stored in permafrost [73]. The nature of SOM and the factors that determine how long it remains in the soil are critical to modeling future carbon dioxide (CO_2) and methane (CH_4) fluxes [6, 39, 65, 67, 142].

In the past two decades, mineral protection of carbon, i.e. carbon physically or chemically attached to minerals such that it is unavailable for microbial decomposition, has been recognized as a critical factor in slowing SOM decomposition [32, 45,

53, 64, 66, 67, 69, 81, 101, 138, 139, 143]. In order to predict how SOM will respond to climate change, accurate models must be developed that consider relevant effects such as how mineral protection interacts with land use and precipitation changes [32, 53, 65, 69, 81, 123, 137, 138]. Iron oxides (including oxihydroxides and hydroxides) are minerals abundant in most soils and have the capacity to protect SOM from decomposition [31, 66, 101]. When conditions are anoxic, as in flooded soils, iron oxides are preferentially reduced (gain an electron) by microbes in order to oxidize organic carbon (which loses an electron) into CO_2 [78, 128]. Hence, iron acts as both an inhibitor and a crucial component of carbon decomposition, but its net impact depends on a suite of complex dynamics that are driven by fluctuations in soil moisture [25, 36, 118, 124, 133]. The motivation behind this thesis is to untangle how hydrological forcings, such as flooding, draining, and random rainfall, affect the iron carbon cycles in soil. Understanding these dynamics mathematically is critical to improving models and predictions of the fate of SOM under climate change, which is expected to alter precipitation patterns across the globe [68].

1.2 Approach

The importance of SOM for agriculture has been known for millennia and studied scientifically for over a century [131, 132]. This has led to the development of different theories and a plethora of models to represent SOM decomposition in the soil, many involving hydrology, microbial populations, and nutrient dynamics (e.g. nitrogen) [84]. Iron and its transformations have also been studied extensively in the soil but largely from a mechanistic point of view, looking at specific processes related to microbiology or geochemistry [19, 46, 79, 107, 108]. Large, complex soil geochemical models can successfully capture iron and carbon cycles, but their complexity makes it difficult to determine fundamental relationships between key variables [21, 110,

122]. Seeking to better understand these core relationships, Calabrese and Porporato (2019) developed a simple model of the coupled iron carbon cycle driven by hydrological fluctuations to parsimoniously model iron reduction and microbial dynamics [22]. Chapter 3 expands on this model, including the role of mineral-associated organic matter (MAOM or mineral-associated organic carbon MAOC). MAOM is protected from microbial decomposition, but may be released if the protecting mineral undergoes dissimilatory reduction [23]. The addition of this pool allows for the contrasting dynamics of iron as a protector and enabler of SOM decomposition to be explored mathematically, which as far as can be determined has not been done before [23, 88, 93, 118, 124, 135, 145].

The availability of iron to protect SOM, oxidize SOM, percolate out of the soil, and be uptaken by plants is dependent on whether its state is reduced (Fe^{2+}) or oxidized (Fe^{3+}) [21, 28, 118, 147]. Thus, the fraction of time iron spends in each of these states is informative for a variety of ecological, mineralogical, and carbon related purposes. Calabrese et al. (2020) built on their aforementioned work [22] by reducing the model to just consider hydrological variables and the fraction of iron that is oxidized or reduced [21]. Chapter 4 of this thesis extends that simplified model by including the impacts of stochastic rainfall. Stochasticity, or randomness, from external forcings has non-linear impacts on a variety of environmental systems when the noise is multiplicative, as it is in this system [99, 102]. By using a simplified model, the probability density function of the state of iron can be found analytically as a function of soil and climatological parameters. The analytical functions are useful (in comparison to numerical simulations) by identifying fundamental relations and tipping points from environmental variables. This ultimately can be used to assess how changing precipitation regimes will interact with iron to affect carbon emissions and iron availability in soil.

1.3 The Challenges of Environmental Models

It would be a failure of due diligence to not discuss, in practical terms, the limitations and plausible objectives of this thesis. The goal of environmental models is generally to best approximate a complex, open system whose true nature is unknowable in its entirety [13]. There are many choices made in modeling, including assumptions, structure of the model, boundary conditions, loss functions/fitting methods, the scale of processes represented, etc. A challenge for many environmental models is equifinality, the phenomenon wherein different sets of boundary conditions, parameters, or model structures fit available data equally well [13, 14]. Ideally, equifinality is addressed with some method that deals with the probabilities of different parameter and model formulations using a large data set, for instance the generalized likelihood uncertainty estimation (GLUE) [15]. An attempt to model the biogeochemical soil system for the sake of prediction is beyond the scope of this thesis and would require a large, complex model that is itself only a macroscopic approximation of reality. Rather, the goal of this thesis is to illuminate the different known mechanisms into a formal model to determine the mathematical relations between variables and their implications for climate change and future modeling endeavors. That is to say, this thesis is not a large-scale data assimilation project to fit models and estimate parameters, but instead aims to examine the effect of different parameters on the iron and carbon cycles via simple, explainable models. Specifically, the models developed can give an idea of what types of conditions/parameterizations will lead to what possible range of outcomes. The parameters in question are (1) the initial conditions and inputs into the system of carbon and iron, and (2) the rates of processes, including the rate of reduction, the rate of oxidation, the rate of decomposition, and rate of switching between oxic and anoxic conditions.

Chapter 2

Literature Review

2.1 The soil carbon cycle

The soil carbon cycle begins when organic matter enters the soil through plant root turnover, root exudates, or above-ground deposition from plants or animals [32, 132]. Once in the soil, it can be considered SOM and is further decomposed by fungi, earthworms, microbes, and other decomposers [32, 132]. During decomposition, decomposers oxidize SOM into mineral products (e.g. CO_2) which are respired into the atmosphere. This energetically-favourable reaction is the source of energy for the decomposers. Not all SOM is decomposed directly into carbon dioxide; some become decomposer biomass, while others remain in the soil as SOM in a slightly altered form [132]. When decomposers die, their necromass becomes SOM available for decomposition [97]. SOM inputs into soil have a wide range of chemical and structural properties which influence the time they take to be decomposed in the soil [82]. Soil properties, such as mineral content, clay content, and microbial populations, also play an important role in SOM decay [101]. The rate of SOM decomposition and the factors that affect it are critical determiners of the net flux of carbon in and out of the soil.

2.1.1 Redox Potential and Decomposition

In the soil, microbes mediate the transfer of electrons from an electron donor (reductant or reducer) to an electron acceptor (oxidant or oxidizer), then trap the energy produced from this favourable reaction [12]. The redox potential of a solution determines how favorable the redox reaction is, and thus whether or not microbes will carry it out. The redox potential of an aqueous solution is highly correlated to its concentration of oxygen gas (O_2). During reactions in oxic conditions (high O_2), oxygen is the dominant electron acceptor for the oxidation of organic matter into CO_2 (aerobic respiration) [12, 111]. However, in soil near water saturation, oxygen is quickly depleted because of its slow rate of diffusion through water [128]. This drastically lowers the redox potential of the soil and causes other oxidizers to be used by microbes. These substitute oxidizers are typically used in order of decreasing redox potential, but this can vary depending on their availability and the soil's pH [12, 111, 128]. The oxidants in the soil with the next-highest redox potential after oxygen are nitrate (NO_3^-), followed by manganese (Mn^{4+}), iron (Fe^{3+}), sulfate (SO_4^{2-}), and carbon dioxide (CO_2), which is reduced to methane at very low redox potentials [12, 111, 128]. Due to the high availability of iron relative to nitrate and manganese, iron becomes a significant oxidizer of SOM during anoxic conditions in many soils [41, 51, 78, 79]. During anoxic conditions, net respiration is usually assumed to decrease because the lower availability of oxygen decreases the thermodynamic potential of decomposition reactions [48, 76]. However, recently it has been observed that flooding increases rates of respiration in some situations [23, 58, 76, 134, 135]. This counterintuitive result suggests that other factors such as the availability of carbon to decomposers must be considered alongside the thermodynamics of soil decomposition [125].

2.1.2 Carbon Stabilization

SOM decays at vastly different rates. The majority of new inputs to the soil decay quickly within a year or two, while other SOM can remain in the soil for decades to millennia [33, 82]. Older carbon comprises the majority of SOM – the mean age of SOM in the soil was estimated by Shi et al. 2020 to be $4,830 \pm 1,730$ years [112]. Understanding the nature of this old, ‘recalcitrant’ carbon will greatly improve predictions of soil carbon fluxes under a changing climate and could lead to improved methods of increasing soil carbon storage via land management [32]. There are several accepted mechanisms that contribute to the storage of carbon, but how they manifest in reality, the relative importance of different processes, and how soil carbon will respond to a changing climate are all critical open questions [32].

The dominant factors perceived to be influencing the rate of SOM decomposition have changed dramatically in recent decades [32, 74, 82]. The accepted paradigm in the 19th and most of the 20th centuries is that the chemical properties of some fraction of SOM made it nearly completely resilient to decomposition [82, 131, 132]. This idea has since been challenged, and a new conceptual model has emerged that considers multiple factors including mineral association, physical accessibility, molecular size, energy content, nutrient ratios, oxidation state, hydrophobicity, number of enzyme steps necessary to degrade, diversity of substrates, and microbial conditions [49, 54, 65, 69, 74, 82, 119, 142]. As noted by [65], the classification of a phenomena, in this case recalcitrant carbon, defines how it is modeled and addressed scientifically. Since prior to the 21st century inherent chemical properties were considered the cause of slow degradation, it was natural to classify SOM based on the degree of lability, meaning how easy it is to decompose [82, 84]. Recently, models have been proposed that centralize other forms of preservation. For instance, models by [138] and [81] demonstrate how including a pool of carbon that is protected from decomposition

by mineral association can produce observed behaviors. Other models, like those of [142] and [87], show how network effects between a large array of microbes who must invest in metabolism and a large diversity of carbon substrates can lead to the preservation of some substrates. The shifting perception of the leading causes of carbon preservation in the soil has led to a new generation of models that reflect these new ideas; of interest to us are the models pertaining to protection via mineral association.

2.1.3 Mineral Association

While several mechanisms contribute to extending the residence time of carbon in soils, abundant evidence suggests that mineral associations are a significant factor in stabilizing organic carbon [32, 53, 66, 82, 139]. MAOM accounts for up to 91% of soil carbon in some soils and has turnover times in the soil on average four times as long as other SOM [66]. MAOM refers to SOM that is adsorbed to (chemically attached to the exterior of) minerals or was coprecipitated with minerals in a metal-organic complex [32, 66]. Mineral adsorption occurs when negatively-charged particles of organic matter interact with the positively-charged surface of minerals. Adsorption and desorption often occur simultaneously at rates determined by the pH, concentration of adsorbed particle in the solution, and strength of bonds formed [66]. Adsorption can be inner-sphere (specific), where polar covalent bonds form between the SOM and mineral, or outer-sphere (non-specific), where long range bonds form but the components remain independent [66]. Outer-sphere electrostatic forces are much weaker than inner-sphere ones [66]. Unlike adsorption, which occurs on the surface of already-formed crystals, coprecipitation occurs when dissolved metal cations interact with organic matter to form complexes that then precipitate into the solid phase [66, 89, 118]. During or soon after this process, more cations or organic matter may adsorb to the coprecipitate, creating larger particles [66, 89]. The extent of ad-

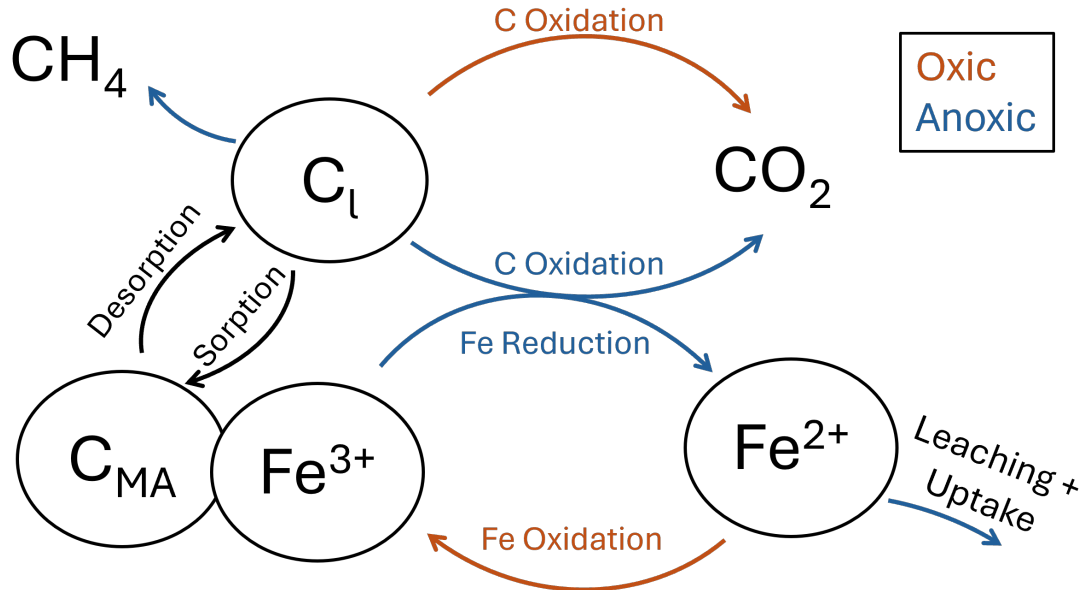


Figure 2.1: The ferrous wheel ($Fe^{3+} \rightleftharpoons Fe^{2+}$) and its interactions with a simplified carbon cycle is shown. Orange arrows are processes that occur in oxic conditions, blue arrows occur in anoxic conditions, and black arrows can occur in both. C_l is used to represent labile, available organic carbon and C_{MA} represents mineral associated organic carbon.

sorption that can occur depends on the available surface area of minerals; however, this limitation is not imposed on coprecipitates which allows for greater Fe-C ratios [Mikutta 2014]. Adsorption is a well-studied process with many existing models to describe its dynamics [96]. In contrast, coprecipitation is more complex and seems to be highly dependent on initial ratios of metal to organic matter in the solution, so there is no consistent model that captures the phenomena [66, 89]. While mineral associations reduce turnover times, it is not necessarily the case that specific MAOM is static for long periods of time [66, 139]. Rather, mineral association is a dynamic process wherein attached carbon may be continuously desorped and adsorbed, partially transformed, or replaced by more strongly-charged organic matter [66, 139].

2.2 The Iron Cycle

Iron, the fourth most abundant element in Earth’s crust, is a key player in soil biogeochemical cycles [28, 31, 63]. Iron is most commonly found in soil in its ferrous (Fe^{2+}) or ferric (Fe^{3+}) forms [31]. The dominant processes in the soil iron cycle are oxidation and reduction. In oxic conditions (high O_2 concentration), Fe^{2+} is oxidized to Fe^{3+} , which then forms iron oxides and precipitates into the solid phase [28, 31]. In anoxic conditions (low O_2 concentration), Fe^{3+} is microbially reduced to oxidize SOM. In highly acidic conditions, chemical abiotic reduction can compete with rates of biotic reduction, but in the pH range of most soils (pH > 4.5), biotic reduction dominates [28, 79, 104]. The rates of oxidation and reduction can both vary by orders of magnitude and depend on environmental conditions and the crystallinity of iron oxides [28, 78, 79, 106, 121]. Iron is also an essential nutrient for all life, including plants. Despite its abundance in most soils, the insolubility of Fe^{3+} makes it limiting to plants, which can only uptake aqueous ions [28]. Fe^{2+} has a much higher solubility than Fe^{3+} ; thus, the redox state of iron can control its availability to plants and leeching from the soil [127].

The iron oxides (including iron oxyhydroxides, hydroxides, and oxides) are widespread iron minerals that have societal (e.g. mining and pigments) and biogeochemical importance (e.g. soil carbon and iron cycles) [31, 66]. The iron oxides are usually formed with (Fe^{3+}), but some like magnetite are composed of both Fe^{2+} and Fe^{3+} [31]. Short-range order, or poorly crystalline iron oxides such as ferrihydrite ($\alpha\text{-FeOOH}$), are considered meta-stable and, if unperturbed, will transform into more crystalline forms, such as goethite via Ostwald ripening [31, 92]. Poorly crystalline oxides have a high specific surface area and thus a high sorptive capacity [28, 31]. Crystalline iron oxides such as goethite ($\alpha\text{-FeOOH}$) and hematite ($\alpha\text{-Fe}_2\text{O}_3$) are more stable and have a lower specific surface area [28, 31]. The properties of iron oxides are im-

portant in the soil iron and carbon cycles because they affect the availability of iron for microbial reduction and the oxides' capacity to associate with SOM [28].

2.2.1 Iron Reduction in Soil

Microbial iron reduction sits at the interface of mineralogy, microbiology, and the carbon cycle [28, 34, 36, 79, 106]. The rate of iron reduction can be influenced by pH, redox potential, electron donors, physical protection, available surface area, electron shuttles, and iron crystallinity [10, 18, 19, 22, 34, 52, 79, 105, 106, 108, 136]. A study by Roden 2003 demonstrated that the thermodynamic stability (Gibbs free energy) of the iron crystal was not the dominant control, but rather, the available surface area of the iron oxide was more important (the significance of thermodynamics has been debated, see [34]) [104]. Processes that decrease the available surface area for reducing bacteria, such as the sorbing of Fe^{2+} , decrease reduction rates [104, 106, 107]. As the reduction of iron oxides progresses, more Fe^{2+} is produced and adsorbs, decreasing the available surface area and reducing reduction rates, leading to a negative feedback loop [10, 107, 108]. If there is advective transport of aqueous Fe^{2+} out of the system, then desorption occurs, leading to the elimination of this feedback loop [107, 108]. However, the formation of secondary minerals with the sorbed Fe^{2+} , such as magnetite, complicates this relationship and can reduce reduction rates even under flow conditions by decreasing the redox potential of the iron mineral [10, 52, 90]. In both non-flow and flow conditions, there is an observed reduction of some fraction of Fe^{3+} minerals, usually poorly crystalline, at a fast rate followed by a sharp slowdown caused by the formation of secondary minerals and/or the sorption of Fe^{2+} , blocking biotic reduction [10, 52, 104, 106]. A major implication of this, as pointed out by Roden 2006, is that short-term reduction rates may be controlled by microbial population, iron oxide stability, and carbon availability, but long-term reduction is controlled by the mass transfer of Fe^{2+} out of the system [106]. Because Fe^{2+} is more

difficult to remove after it mineralizes, it may be the case that the rate of advection compared to the rate of mineralization is a key ratio controlling iron reduction and mass balance in soils [56, 90].

Other factors, including pH and the adsorption of SOM, can also influence iron reduction rates in the soil. The association of SOM with iron oxides (i.e. MAOM) has been shown to both increase and decrease reduction rates. On one hand, MAOM adsorption reduces available surface area, decreasing reduction [5, 36]. On the other hand, MAOM can serve as an electron shuttle, increasing reduction [3, 36]. Iron reduction becomes more energetically favorable with decreasing pH because it consumes protons [85]. However, the impact of pH is not clear, because decreasing pH can also increase sorption which affects reduction rates [5, 36, 140]. The acidity of the soil can also influence which microbes thrive, thereby indirectly affecting iron reduction rates [60]. While much is known about iron reduction, the complexity of soil means that currently-viable macroscopic models only capture broad strokes without considering microscale dynamics [56].

To summarize, SOM and Fe^{2+} adsorption, mineral structure, pH, and the microbial community are all major influences on the rate of reduction, which can vary by orders of magnitude in soils [36, 62]. The most quickly reducible forms of iron are short-range order, poorly crystalline iron oxides that have a large specific surface area [106]. The large surface area of these oxides causes them to sorb more SOM, making them particularly relevant for carbon stabilization [127]. The differences in surface area between types of minerals combined with the impact of negative feedback effects from sorption creates two pools, a quickly-cycling pool and less-easily-reducible stable pool. The reduction rate of the fast pool is dependent on biogeochemical factors, while the reduction of the slow pool is likely dependent on the rate of iron mass transfer out of the system through leaching [106, 127].

2.2.2 Iron Oxidation

The oxidation of ferrous iron (Fe^{2+}) into iron oxides is energetically favourable in oxic conditions. The crystals formed during oxidation depend on environmental conditions, including SOM content, pH, and speed of oxidation [126, 127]. In soils, abiotic oxidation is often assumed to dominate microbial, especially at neutral or alkaline pH [28, 38]. Microbially-mediated iron oxidation has been observed in rainforests and streams, but it is assumed to be slower than abiotic oxidation [37, 38]. Besides redox potential, pH is a dominant controller of iron oxidation [116, 121]. Singer and Stumm (1970) found that oxidation rate is proportional to the square of the concentration of hydroxide (OH^-), i.e. for a unit increase in pH, the oxidation rate should increase by two orders of magnitude [116, 121]. Iron oxidation may also play a role in SOM decomposition by producing reactive oxygen species that then oxidize SOM [51]. Iron oxidation is critical for the formation of various iron oxides that are ubiquitous in soils. Unlike reduction, which is microbially dominated in soils, iron oxidation is often assumed to be abiotically dominated in which case its rate depends only on the redox potential and pH of the soil.

2.3 The Coupled Water-Iron-Carbon Cycles

While it has been mentioned in the previous sections, it is vital to emphasize the processes coupling the water, iron, and carbon cycles. When soils are not saturated, conditions are generally oxic and SOM is oxidized by oxygen. In oxic conditions, iron is present as Fe^{3+} in iron oxides [31]. These oxides, particularly short-range order, poorly crystalline oxides with a high surface area, adsorb SOM or are complexed with it from coprecipitation [66]. When SOM is attached to minerals, it becomes MAOM, which is protected from most microbial decomposition [66]. This protection has important global implications for the ability of the soil to store carbon under

climate change [24, 32, 45, 53, 123].

At high soil moistures (above field capacity, when leakage is significant), oxygen concentration drops precipitously, leading to anoxic conditions [128]. In anoxic conditions, SOM decomposition occurs more slowly because other oxidizers have lower redox potential than oxygen [12, 128]. Ferric iron (Fe^{3+}), due to its abundance and relatively high redox potential, is often the most significant oxidant in anoxic conditions [2, 28, 36, 78, 118]. The rate of reduction is impacted by soil carbon via the carbon sorbed to iron oxides, the population of microbial reducers, and the amount of carbon available for reduction [22, 88, 89]. The reduction of iron oxides releases the carbon stored on it, in turn releasing protected SOM to become available for decomposition [23, 58, 88, 93, 95, 135]. This effect has been shown in field studies and lab experiments to increase the amount of carbon available for decomposition [23, 58, 88, 93, 95]. Iron reduction can have secondary effects on SOM decomposition as well by impacting pH and/or enzyme activity [135]. The production of ferrous iron (Fe^{2+}) can reduce the enzyme phenol oxidase in wetlands which can inhibit SOM decomposition [135].

Fluctuations in soil moisture drive complex dynamics between iron and carbon with non-obvious effects. Understanding the dynamical system at play is critical to improving models of how stored organic carbon will react to changing climactic conditions and rainfall patterns [32, 123]. One of the most critical questions is what the impact of iron on the carbon cycle is over different time scales [118]. Short anoxic periods (days to weeks) may reduce the amount of carbon respired by decreasing the rate of SOM decomposition [128]. Long anoxic periods (e.g. seasonal flooding), however, may lead to the release and decomposition of previously mineral associated organic matter, increasing the amount of carbon dioxide or methane released. This effect was shown by Huang and Hall 2017 in a 150-day wetland experiment, suggesting that iron-carbon dynamics should include mineral protection and dissolution [58].

While these processes are understood mechanistically, without modeling it is difficult to parse the influence of feedback effects, non-linear dynamics, and tipping points that may play key roles in the system.

2.4 Modeling Soil Processes

The previous sections gave a broad overview of important mechanisms that lead to the net macroscopic effects of the soil carbon and iron cycles. This section aims to cover how these processes are modeled mathematically. The goal of the models used and discussed in this thesis is not to represent every detail of the system, but to connect a quantitative framework with an understanding of the major processes to untangle the relations between important variables and processes. With that in mind, this section will begin with an overview of existing compartment models, also known as pool models, and show how they have been used to model soil moisture, SOM, and the iron cycle.

2.4.1 Compartment Models

Models of many environmental and physical systems, including many SOM models, are compartment models [42, 84, 113]. There are two necessary elements of a compartment model. The first is a quantity or variable of interest. The second are the fluxes, or inflows and outflows, of the system. Employing the conservation of mass, change in storage over time must equal inflow minus outflow. Mathematically, this can be represented as

$$\frac{dx}{dt} = I - O, \tag{2.1}$$

where $\frac{dx}{dt}$ is the change in storage, I is inflow, and O is outflow. Compartment models can be used to describe physical, concrete quantities, such as the volume of water in a lake, or functional groups, such as the population of infected individuals during a

pandemic [30]. This model can be naturally extended by adding more pools, which we can represent by a vector, $\vec{x} = (x_1, x_2, \dots, x_n)$. This yields the following equation:

$$\frac{d\vec{x}}{dt} = \vec{I} - \vec{O}, \quad (2.2)$$

which is a system of n ordinary differential equations (ODEs). If the fluxes of the state variables depend on each other ($I_i(x_j)$), then the equations are coupled and together make a dynamical system. If the system is linear, meaning that each flux is only a linear function of itself or other state variables, then it can be solved analytically. If this is not the case, then the equation cannot be solved analytically, but the steady state solution may be possible to find by setting the time derivatives to zero [83, 113]. Non-linear dynamical systems can be run numerically in order to investigate the dynamics [113]. Compartment models have long been used to model SOM dynamics and will be used throughout this thesis to represent water and different forms of iron and carbon within the bounds of the soil [84].

2.4.2 Soil Moisture Models

Soil moisture is a key variable in SOM decomposition and the most important factor in the iron cycle [22]. It is the medium in which nearly all soil interactions happen, and it controls the redox potential, plant productivity, and leeching of solutes [99]. Soil moisture primarily flows vertically, and many models include the vertical direction in their formulation [84, 147]. However, a simple compartment model where the variable of interest is the vertically-averaged volume of water in the soil-rooting zone (\approx top 40 cm) can be a good approximation, capturing most of the important dynamics [99]. In such a model, the state variable is the relative soil moisture, s , defined as the volume of water divided by the total volume of pores in the soil. The fluxes out of the soil include evaporation ($E(s)$), transpiration ($T(s)$), leakage ($L(s)$), and runoff

($Q(s)$), which are all functions of soil moisture [99]. The only input is infiltration ($I(t)$), defined as rainfall minus canopy interception. Because rainfall occurs quicker than the length of a typical drydown, an approximation can be made that rainfall occurs instantaneously [99, 109]. Therefore, the governing ODE can be written as

$$nZ_r \frac{ds}{dt} = I(t) - Q(s) - L(s) - ET(s), \quad (2.3)$$

where n is the porosity of the soil and Z_r is the rooting depth. Equation (3.1) can be related back to (2.1) by simply letting $x = snZ_r$; inflow is still I , and outflow is the sum of runoff, leakage, and evapotranspiration ($O = Q + L + ET$). The details of the functions can be found in section 3.1. One benefit of this compartment model is that it can be intuitively understood while still being loyal to the underlying physics. The other benefit is that stochastic rainfall can be added to determine important statistical information about soil moisture [99, 109].

2.4.3 Iron Cycle Models

Chemical reactions are often modeled using ODEs that can be reframed as compartment models. The state variables, or compartments, are the masses of a given reactant or product that change in time with rates proportional to the concentration of reactants. A reaction is said to be first-order if its rate of change depends only on its own concentration, for instance the decay of an unstable isotope. A first-order decay reaction has the form:

$$\frac{dx}{dt} = -kx. \quad (2.4)$$

where the decay is proportional to the mass of the substance x times a rate constant k . When a reaction depends on the concentration of two reactants, it is second-order, but if one reactant is much more limiting than the other, it can often be reduced to a first order reaction with respect to the rate limiting reactant. For example, abiotic

iron oxidation depends on O_2 and Fe^{2+} , but in oxic conditions O_2 is expected to be at saturation and roughly constant relative to Fe^{2+} . Thus, the oxidation of Fe^{2+} can be approximated by:

$$\frac{dFe^{2+}}{dt} = -k_o Fe^{2+}, \quad (2.5)$$

where k_o is an oxidation rate constant. This assumption is only valid if the conditions are oxic and oxygen is abundant. To account for changing soil moistures and redox states, a term may be amended that is a function of soil moisture to represent shifting redox conditions.

Iron reduction is typically coupled to the oxidation of SOM and carried out by microbes. Microbially-mediated reactions are typically modeled using Michaelis-Menten kinetics which takes into account the role of enzymes that catalyze the reaction. Ginn et al. 2017 model iron reduction using this type of reaction with an equation of the form

$$\frac{dFe^{3+}}{dt} = -k C_{BM} \frac{Fe^{3+}}{K_m + Fe^{3+}}, \quad (2.6)$$

where k is the reaction rate constant in units of Fe^{3+} per unit biomass, K_m is the Michaelis-Menten half saturation coefficient, and C_{BM} is the concentration of microbes [46]. The main difference between Michaelis-Menten and linear reactions is that there is a saturating effect at high concentrations of the substrate. In equation (2.6), for $x \gg K_m$, the rate approaches $\frac{V_{max}}{K_M}$ which is zero-order. For low concentrations of substrate, the rate approaches first-order kinetics. In some instances, it is convenient to assume reactions are first order as they have nicer mathematical properties and this assumption usually does not qualitatively change the dynamics. Another model of reduction, proposed by Calabrese and Porporato 2019, represents iron reduction with the following equation:

$$RED = -k_r C_{BM} C_I Fe^{3+}, \quad (2.7)$$

where C_{BM} is the population of microbial biomass, C_1 is the concentration of available carbon to oxidize, and k_r is a rate constant. Similarly to oxidation, a function of soil moisture is amended to account for the redox potential of the soil [22]. Equation (2.7) differs from (2.6) by including the impact of the electron donor (C_1) and linearizing the Michaelis-Menten kinetics. The models considered here are macroscopic representations of countless serendipitous collisions between microbes, reductants, and oxidants on the microscopic scale. There is no single right way to model these processes; rather, variables of interest are selected to based on the purpose of the model and resolution it seeks to capture.

2.4.4 Carbon Cycle

The soil carbon cycle is often represented using a compartment-based model. As opposed to the iron cycle which uses the oxidation state as a compartment, carbon models are often grouped by functionally similar pools, which can encompass a diverse array of chemical compositions [84]. The formerly accepted paradigm of SOM decay was that the rate of decay is based on inherent chemical properties of the SOM. Because of this conception, functionally similar groups were defined as those that have similar decay times [82, 84, 113]. Chemical SOM recalcitrance has greatly influenced the development of models over time, and several currently used models are still based on these dynamics [81, 123]. The decay functions of these pools can be complex functions of several variables or simple first-order decays. The first-order decay model for SOM was first proposed by Olson 1963 [91, 113]. The following example is a model with two pools, labile carbon (C_l) and humic, or recalcitrant, carbon (C_h) undergoing first-order decay with no inputs.

$$\begin{aligned}\frac{dC_l}{dt} &= -k_l C_l \\ \frac{dC_h}{dt} &= -k_h C_h.\end{aligned}$$

First-order decay models do not include microbial processes but can still fit data well, especially if multiple pools are included [84]. The model of equation (2.8) can be extended to include n pools all undergoing decay, where the fraction of initial OM added to each pool sums to one. If this were extended to the limit where the number of pools n approaches infinity and the proportion of new OM in each pool approaches zero, then it becomes the special case of a continuous quality model, first proposed by Agren and Bosatta 1998 [4, 84, 113]. Equation (2.8) can also be expanded, for instance, by putting the models in series to represent exchange between pools. Or, a microbial biomass pool could be introduced that represents cycling between microbes and SOM [84, 97]. Each of these possibilities represents a different dynamic, but these complications come with drawbacks [84, 113]. As models become more complex, their cycles are more difficult to understand, and analytical solutions become impossible or intractable. For an overview of the plethora of models describing SOM decomposition and their mathematical descriptions, see Sierra et al. 2015 and Manzoni and Porporato 2009 [84, 113].

As the conception of SOM has shifted to be broader, placing a larger emphasis on mineral association, spatial accessibility, and microbial thermodynamics (i.e. is it energetically worth it for microbes to decompose certain SOM), models have begun to incorporate these dynamics; however, much work remains to be done [75, 81, 142]. In a 2017 paper, Luo et al. create a model to show how the protection of SOM via mineral association or physical occlusion can explain carbon recalcitrance in the soil just as well as a model based on ideas of chemical recalcitrance. The chemical recalcitrance model followed equation (2.8), where one pool is quickly decomposing, the other pool is slowly decomposing, and there is no exchange between the two. The protection model used two pools, one to represent available, unprotected carbon (C_u) and the other to represent protected carbon (C_p) that is completely unavailable for

decay. The dynamics are expressed mathematically as

$$\frac{dC_p}{dt} = -g_p(p_{max} - C_p)C_u - I_pC_p \quad (2.8)$$

$$\frac{dC_u}{dt} = k_uC_u - g_p(p_{max} - C_p)C_u + I_pC_p. \quad (2.9)$$

$g_p(p_{max} - C_p)C_u$ is a term representing unprotected carbon gaining protection, which reaches saturation at p_{max} . I_pC_p represents the rate at which protection is lost, and k_uC_u represents decay of unprotected carbon. Luo et al. 2017 found that the different models can similarly explain observations but lead to drastically different predictions of current carbon stores and decomposition dynamics [81]. A more applied version of the protection model was developed by Woolf and Lehmann 2019 and includes five carbon pools for soluble plant matter, insoluble plant matter, dissolved organic carbon, mineral associated carbon, and carbon in microbial biomass [138]. This model, also with no slow-cycling pool, was also able to successfully explain long term carbon persistence [138].

2.4.5 Modeling the Coupled Water-Iron-Carbon Cycle

To capture the rich dynamics of the carbon and iron cycles, the cycles have to modeled simultaneously with each other and with soil moisture. A dynamical system combining the models previously discussed is necessary. Large-scale biogeochemical models may incorporate all of these dynamics, but their complexity limits the ability to draw conclusions about the specific effects of this coupling [11, 22]. A simple model coupling hydrology, iron, and carbon cycles was developed in 2019 by Calabrese and Porporato, who modeled the system using a pool for Fe^{3+} , Fe^{2+} , non-biomass carbon, and microbial biomass [22]. The equations were coupled via the reduction term (equation (2.7)), a linear function of microbial biomass, available carbon, and Fe^{3+} multiplied by a function that related soil moisture to redox potential [22]. The sys-

tem, although simple, reproduced a plausible phase space of Fe^{2+} and soil moisture for data collected by Barcellos et al. 2018 in a tropical rainforest [7]. Models including more factors, such as pH, competition with methane producing bacteria, and temperature, were developed by Zheng et al. 2018 and Sulman et al. 2022 to look at the impact of iron reduction on the dynamics of arctic fens, which are growing rapidly due to melting permafrost [124, 146]. They found that non-linear pH effects can significantly impact results versus models that do not use them in wetlands [124, 146].

From the carbon modeling side, some existing models incorporate mineral protection [81, 138]. These models, however, do not take into account the changing availability of iron minerals in the soil, which reduce the protection offered. They also do not explicitly include iron cycle dynamics. There is a gap between these two fields, where models focused on SOM protection do not include changing redox conditions, and models including changing iron reduction do not include carbon protection. These two effects interact and combined determine whether or not hydrological fluctuations will lead to increased or decreased carbon respiration. Chapter 3 of this thesis develops a model incorporating mineral protection, changing mineral availability, and iron as an oxidant to untangle the dynamics of the coupled iron-carbon cycle under different hydrological regimes.

2.5 Stochasticity in Environmental Models

As established, the soil cycles have several moving parts that all interact over many timescales. Further complicating this, soil moisture is highly variable with impulses of precipitation from a chaotic weather system that is virtually random from the point of view of the soil [109]. The role of randomness, stochasticity, or noise is ubiquitous in environmental systems and can originate from rain, animals, fires, nutrient inputs,

or turbulence amongst other phenomena [102]. When noise is additive, a general equation can be written using the following stochastic differential equation (SDE):

$$\frac{dx}{dt} = f(x) + \varepsilon(t). \quad (2.10)$$

In this case, the noise can dominate the system if the signal $\varepsilon(t)$ is much greater than the effect of the deterministic dynamics $f(x)$ or be negligible if the amplitude of the noise $\varepsilon(t)$ is small relative to $f(x)$ [102]. In the first case, the system becomes dominated by stochasticity, and in the second case, the dynamics are not qualitatively changed. However, if the noise is multiplicative, entirely new and rich behaviors can emerge [35, 102]. A general equation of multiplicative noise is

$$\frac{dx}{dt} = f(x) + g(x)\varepsilon(t), \quad (2.11)$$

where the multiplication of $g(x)$ and the noise term can often qualitatively change the behavior of the system. An in depth overviews of noise in environmental systems can be found in the book by Ridolfi et al. 2011 [102], and an overview of stochasticity particularly as it pertains to various soil moisture topics can be found in Porporato and Yin 2022 [99].

The effect of noise on a model can be studied in two ways: numerically or analytically. Most stochastic environmental systems are too complex to be solved analytically and their dynamics are determined by running Monte-Carlo simulations with randomly generated noise representing some environmental fluctuation (e.g. random rainfall) [130]. The result of such a simulation may be a histogram of the value of the state variable x after a simulation of length T . This histogram, as the number of runs becomes sufficiently large, will approach the probability distribution function (PDF), $p_X(x)$, of x at time T . The notation used here is that lowercase x is a deterministic value representing a specific value, while capital X represents the random

variable that is not described by a constant but by the PDF, $p_X(x)$. $p_X(x)$ represents the probability that X is equal to x (or technically that X is within a small interval $x \pm dx$).

The other way to study stochastic systems is to derive the steady state PDF and, if possible, the trajectory of the PDF over time [102]. The steady state PDF of SDEs can be found for specific known cases, many of which have environmental applications [102]. The advantage of analytical solutions is that the impact of different variables on the steady state dynamics are readily apparent, and important information, including the mean, tipping points, singularities, and relations between variables can all be derived [102]. Analytical methods of studying noise-driven environmental systems have been applied to climate resonance, soil moisture, ecosystem dynamics, spatial vegetation patterns, food chain ecology and more [102]. In this thesis, a numerical, Monte-Carlo simulation is employed to study the iron-carbon model (following Calabrese and Porporato 2019), while analytical methods are used to study the dynamics of a simplified iron system driven by random redox fluctuations [22].

2.6 Summary

The iron and carbon cycles are coupled by several mechanisms that depend on the redox state of the soil, which in turn depends on soil moisture. The first important mechanism is the microbial reduction of iron oxides to oxidize organic carbon [80, 118]. Due to its abundance and favorable redox potential, iron oxides can be a significant driver of SOM decomposition in anoxic soils [78, 118, 124]. The second important mechanism is the stabilization of SOM in the soil by association with iron-oxides, estimated to be a significant controller of carbon turnover time in the soil [32, 53, 66, 82]. These processes intersect when the dissimilatory reduction of iron oxides frees the previously-attached organic carbon, a phenomena that has been observed

in multiple studies [23, 58, 88, 93, 95, 135]. Existing models look at both of these phenomena separately [22, 81, 124, 138], but as far as can be determined, no models have explicitly looked at the impact of both concurrently and the consequences of this for the iron-carbon cycle.

Compartment models are a simple yet wide-ranging and effective tool to model dynamical environmental systems [42]. Models are vital to understand the long-term impacts of climatological changes (e.g. changing rainfall patterns) on soil carbon decomposition [123]. Currently, soil carbon models diverge in their predictions of the effect of climate change on carbon stocks due to the ways in which carbon stabilization in the soil is modeled [123]. This thesis considers the stabilizing and destabilizing effect of iron on carbon under varying conditions and hydrologic fluctuations. Further complications arise from the role of noise, which can significantly impact the behavior of dynamical systems, such as the iron-carbon cycle, when it applies multiplicatively [102]. To address noise, both numerical and analytical methods can be employed. This thesis finds a novel, analytical steady-state solution for the distribution of iron in soils, addressing the impact of stochastic fluctuations of soil moisture for the first time. This solution serves to illuminate the key variables that control the presence of iron in its oxidized or reduced form, which is relevant to both the iron cycle through plant uptake and leaching and the carbon cycle via reduction rates and mineral protection capacity.

Chapter 3

A Numerical Model of the Water-Iron-Carbon Cycles

3.1 Bucket Soil Moisture Model

Soil properties, including pore size distribution, depth, and the abundance of roots influence the hydrologic regimes of a soil [99, 109]. Here, following Laoi et al. 2001 a non-dimensional bucket model is used to represent the soil. By vertically average over the rooting depth, Z_r , the model complexity is greatly reduced while important effects and plant dynamics are retained. This bucket model has been used in a variety of previous soil water balances and biogeochemical models [22, 71, 84, 97, 99, 109]. The input of water to the model is infiltration, $I(t)$, which is assumed to occur instantaneously during rainfall. If the rainfall exceeds the capacitance of the soil, the rest is assumed to runoff [71, 109]. Percolation, or leakage, $L(s, t)$, is a function of soil moisture and soil properties and is the most important loss term near saturation, when hydraulic conductivity $K(s)$ is high, and becomes negligible below field capacity, s_{fc} . Evaporation and transpiration, $E(s)$ and $T(s)$ respectively are also modeled as functions of soil moisture and are the dominant losses at intermediate soil moisture

[71, 109]. In this thesis, many plant dynamics are not explicitly represented, such as increased transpiration during the day, allowing transpiration to become only a function of soil moisture. Together, these equations yield a governing equation

$$nZ_r \frac{ds}{dt} = I(t) - L(s) - T(s) - E(s). \quad (3.1)$$

With

$$L(s) = \frac{K_s}{\exp \beta(1 - s_{fc}) - 1} (\exp \beta(s - s_{fc}) - 1), \quad (3.2)$$

where K_s is the saturated hydraulic conductivity, $\beta = 2b + 4$ where b is the pore size distribution index, and s_{fc} is field capacity [71].

$$E(s) = \left\{ \begin{array}{ll} 0 & 0 \leq s \leq s_h \\ \frac{s-s_h}{s_w-s_h} E_{max} & s_h < s \leq s_w \\ E_{max} & s_w < s \leq 1 \end{array} \right\} \quad (3.3)$$

and

$$T(s) = \left\{ \begin{array}{ll} 0 & 0 \leq s \leq s_w \\ \frac{s-s_w}{s^*-s_w} T_{max} & s_w < s \leq s^* \\ T_{max} & s^* < s \leq 1 \end{array} \right\}. \quad (3.4)$$

Where E_{max} and T_{max} are maximum soil evaporation and maximum transpiration respectively. The parameters obey the order: $s_h < s_w < s^* < s_{fc}$, which are the soil hygroscopic point, the wilting point, the stress point, and field capacity respectively [71].

3.1.1 Rainfall Modelling

Following work by Rodriguez-Iturbe et al. 1991 and Laio et al. 2001, rainfall incidents are modeled as a Poisson process with rate of λ in units of [1/day] [71, 109]. This stochastic process arises if one first assumes that rainfall is equally likely at every

instant, with a mean frequency of falling equal to $1/\lambda$. The probability distribution function (PDF) of time between rainfalls, τ , is an exponential with expected value (mean) $\mathbf{E}[\tau] = 1/\lambda$, which is written as

$$p_T(\tau) = \lambda e^{-\lambda\tau} \quad (3.5)$$

The depth of rainfall is also modeled as an exponential distribution, with mean depth α . The mean depth of rain, h , has a distribution:

$$p_H(h) = \alpha^{-1} e^{-\frac{h}{\alpha}}. \quad (3.6)$$

This mathematical representation is extremely useful in allowing for the calculation of the soil moisture probability [71, 109]. The product, $\alpha\lambda$, is equal to the mean daily rainfall in a given system. Multiplying this number by 365 days/year gives the mean annual rainfall, a commonly used statistic for classifying ecosystems [55].

3.2 Iron Cycle

To model the coupled iron and carbon cycles we use a dynamical system composed of a series of ordinary differential equations. While the interactions between the iron cycle and carbon cycles are quite complex, the relationships this model focuses on are the role of iron as a substitute electron acceptor in anoxic conditions and the role of iron oxides in protecting mineral associated carbon (C_{MA}) [3, 18, 19, 22, 23, 28, 36, 51, 58, 62, 64, 70, 93, 95, 118, 139, 144, 145]. The equations governing the iron cycle are as follows

$$\frac{d\text{Fe}^{2+}}{dt} = MW - L_{Fe}(s) - UP(s) - \text{OX} + \text{RED} \quad (3.7)$$

$$\frac{d\text{Fe}^{3+}}{dt} = \text{OX} - \text{RED}. \quad (3.8)$$

Where Fe^{2+} is the reduced phase of iron that is more aqueous and thus vulnerable to leakage ($L_{Fe}(s)$) and uptake by plants ($UP(s)$). This system only considers the redox active iron oxides, which is mainly the short-range order, poorly crystalline oxides with a large specific surface area. This pool is more easily available for reduction and cycles faster. Exchange between the redox active pool and the stable pool of iron is an interesting question that has been shown to depend on leaching rates, but will not be explored in this thesis [106, 120]. The equations for OX and RED are adapted from Calabrese and Porporato 2019 and are dependent on the redox state of the soil, which is assumed to be directly controlled by soil moisture. The OX term represents abiotic oxidation in oxic conditions and only depends on soil moisture and Fe^{2+} population, it is written as a first order decay

$$\text{OX} = k_{ox}\text{Fe}^{2+}g(s). \quad (3.9)$$

k_{ox} is a rate constant in units of [1/d]. The equation for reduction is proportional to the iron available (Fe^{3+} and the available electron donors which is assumed to be available organic carbon (C_l)). This yields a reduction equation of

$$\text{RED} = k_{red}\text{Fe}^{3+}C_l f(s). \quad (3.10)$$

Here, the dependency on microbial population used in Calabrese and Porporato 2019 has been dropped [22]. Assuming no dependence on microbes is common practice in SOM decomposition, and it is used here to reduce the number of dimensions of the system [84]. The functions $g(s)$ and $f(s)$ represent the dependence of the processes on redox conditions and thus soil moisture. These equations, also from Calabrese and Porporato 2019 are

$$f(s) = \begin{cases} 0 & s < s_{fc}, \\ \left(\frac{s-s_{fc}}{1-s_{fc}}\right)^\beta & s \geq s_{fc} \end{cases} \quad (3.11)$$

$$g(s) = \begin{cases} 1 & s < s_{fc}, \\ 1 - \left(\frac{s-s_{fc}}{1-s_{fc}}\right)^\varepsilon & s \geq s_{fc} \end{cases} \quad (3.12)$$

The leakage and uptake terms ($L_{Fe}(s)$ and $UP(s)$) are directly proportional to soil moisture leakage and plant transpiration respectively.

$$L_{Fe}(s) = L_{Fe}(s)[Fe^{2+}] = L_{Fe}(s)\frac{Fe^{2+}}{snZ_r} \quad (3.13)$$

and

$$UP(s) = T(s)[Fe^{2+}] = T(s)\frac{Fe^{2+}}{snZ_r}. \quad (3.14)$$

In the above equations $[Fe^{2+}]$ is the concentration of Fe^{2+} in g/volume water/kilogram dry soil where the product of soil moisture (s), porosity (n), and rooting depth (Z_r) represents the volume of water.

3.3 Carbon Cycle

The functional groups of carbon this model focuses on are available (labile) organic carbon (C_l) and mineral associated (protected) organic carbon (C_{MA}). The interactions between these pools are driven by soil moisture fluctuations and the iron cycle, represented by the following ODES

$$\frac{dC_l}{dt} = ADD - DEC_{aer} - DEC_{Fe} - DEC_{CH_4} - SRP + DSRP \quad (3.15)$$

$$\frac{dC_{MA}}{dt} = SRP - DSRP \quad (3.16)$$

The only input to the soil organic carbon is via ADD which represents plant litter from processes including leaf fall, plant death, and root exudation. The only path for carbon to leave the system is via respiration of carbon dioxide or methane, which

is represented by the DEC terms. Decomposition can either be aerobic (DEC_{aer}), anaerobic and iron utilizing (DEC_{Fe}), or anaerobic and methane produce (DEC_{CH_4}). DEC_{Fe} is proportional to the reduction of iron, $DEC_{Fe} = \Omega RED$ where Ω is a term representing the grams of carbon oxidized per gram of carbon reduced. This number is estimated to be $\Omega = 0.054$ from an assumed molar ratio of 4 mol iron needed to oxidize 1 mol carbon [22, 123]. The aerobic decomposition, DEC_{aer} , is modeled as first order decay modified by soil moisture as [97]

$$DEC_{aer} = k_{aer} C_l g(s). \quad (3.17)$$

Similarly, methanogenesis is modeled as a first order decay modified by the soil moisture function $f(s)$ as

$$DEC_{CH_4} = k_{CH_4} C_l f(s). \quad (3.18)$$

In these equations $f(s)$ and $g(s)$ are the same as those used in reduction and oxidation (equations (3.11) and (3.12)). k_{aer} and k_{CH_4} are rate constants with units [1/day], where k_{CH_4} is much lower than k_{aer} due to the reduced efficiency of the reaction.

3.3.1 Mineral Association

Mineral associated carbon reflects a variety of attachment methods including direction sorption, co-precipitation, and aggregation [3, 52, 139]. These will be represented using a sorption equation following Luo et al. 2017 [81]

$$SRP = k_{srp} (\omega Fe^{3+} - C_{MA}) C_l \quad (3.19)$$

$$DSRP = k_{dsrp} C_{MA}. \quad (3.20)$$

where k_{srp} and k_{dsrp} are rate constants for sorption and desorption in units of [1/day] and ω is the ratio of mass carbon adsorbed per gram of reactive iron. ω was found

to vary between 0.05 and 3.8 grams C per gram Fe in US forest soils [144].

3.4 Steady State Analysis

One of the major questions around carbon protection in the soil is what factors or processes matter the most in prolonging carbon storage in the soil [125]. Thermodynamic limitations, mineral association, and other factors all play a role, but untangling their impact quantitatively in different soil systems is difficult [125]. The goal of this section is to compare the turnover time of carbon in permanently anoxic soil to permanently oxic soil using the simple system developed. Carbon age, transit time, and turnover time are often confused terms [114]. Turnover time is defined here as the ratio between the volume or mass of carbon in the soil divided by the out flux at steady state. When dynamical systems can not be solved analytically, as is the case here, the steady-state analysis can provide useful information on the behavior of the system in the long term. Due to the external driver of the system, hydrological fluctuations, the system can only be solved in steady state at constant soil moisture. To find the steady state behavior the time derivatives of the system, equations (3.8) (3.7) (3.15) and (3.16), are set to zero and the system is solved algebraically.

In the anoxic case ($s = 1$) the steady state is straightforward. All of the iron is reduced into Fe^{2+} and a balance is reached between mineral weathering and losses from leakage and uptake. Because there is no reactive iron, C_{MA} approaches 0. The only out flux remaining for C_l is anaerobic decomposition, DEC_{CH_4} . Setting the time derivative to zero yields $C_l^s = ADD/k_{CH_4}$.

In the oxic case all of the iron is in its oxidized form (Fe^{3+}). By summing the state equations for C_l and C_{MA} , it can be derived that $C_l^s = ADD/k_{aer}$. The steady

state C_{MA} can then be solved for to yield

$$C_{MA}^s = \frac{k_s C_l^s \omega \text{Fe}^{3+}}{k_d + k_s C_l^s}. \quad (3.21)$$

By dividing C_l by $C_{MA} + C_l$ one can determine the proportion of carbon that is protected at steady state in oxic conditions. In determining whether or not oxic conditions 'preserve' SOM in the soil for a longer time, the turnover time, T can be a useful metric. In oxic conditions, the system simplifies to unprotected/protected system proposed in Luo et al. 2017 [81]. Because influx = out flux at steady state, the out flux for carbon is simply equal to the rate of addition, ADD . In anoxic conditions the turnover time, T_a , can be calculated to obtain

$$T_a = \frac{ADD/k_{CH_4}}{ADD} = \frac{1}{k_{CH_4}}. \quad (3.22)$$

In oxic conditions, the total volume of C in the soil is the sum of labile and mineral associated carbon which yields a turnover time of

$$T_o = \frac{C_l^s + \frac{k_s C_l^s \omega \text{Fe}^{3+}}{k_d + k_s C_l^s}}{ADD} = \frac{1}{k_{aer}} + \frac{k_s \omega \text{Fe}^{3+}}{k_d k_{aer} + k_s ADD}. \quad (3.23)$$

Equation (3.23) is a modified turnover time of a simple one pool model with a decomposition rate k_{aer} . In the absence of iron protection (e.g. Fe^{3+} or ω go to 0), it reduces to this one pool model. In the no iron case, because $k_{CH_4} < k_{aer}$ one finds that $T_a > T_o$. In this case the thermodynamic limitations of anoxia reduce the decomposition rate and increase the carbon storage potential of permanent wetland soils. This agrees with current knowledge on why wetlands are sinks of carbon [125]. In the case where iron protection is significant, the turnover time increases linearly with the available protection, ωFe^{3+} . It can also be noted that oxic turnover time, equation (3.23), decreases with increasing addition rates of SOM, not visible in the

no-protection or anoxic case. This suggests that the priming effect may be in part explained by mineral association, which is when SOM addition increases the rate of decomposition of existing SOM in the soil [43, 94]. This was observed numerically by Luo et al. 2017, but is shown here for the first time analytically [81].

3.5 Model Set Up

The model is run numerically using a forward Euler approximation. The derivative of a quantity x with respect to time is approximated as

$$\frac{dx_i}{dt} \approx \frac{x_{i+1} - x_i}{\Delta t}, \quad (3.24)$$

where x_i is the value of x at time step i , and Δt is a constant chosen as the time step so as to ensure stability. The code was implemented in python and the time step used throughout was $\Delta t = 1/100\text{d}$.

To run the model under different scenarios it must be parameterized and the initial conditions must be given. Typically models are parameterized using outside information or data. In terms of data availability, there are several studies investigating the rate of iron reduction under different conditions [3, 19, 46, 51, 79, 80, 108]. A few controlled experiments have investigated the impact of iron reduction on the release of carbon [23, 88, 93]. There are some field studies that implicitly include both effects by observing changes in iron and carbon under different hydrological regimes [58, 95, 134, 135]. Fitting to a single set of data would give a single, diagnostic model, which can only be applied locally [15]. Instead, this model is applied over a range of parameter values to demonstrate the breadth of the modeling space [15] and the possible interactions between parameter values and hydrologic regimes as it pertains to carbon emissions.

3.5.1 Parameterization

The model is based on that of Calabrese and Porporato 2019 and so their parameter values are used as a starting point; the full list of parameters can be found in table 3.1 [22]. The soil parameters will be kept constant and are based on Luquillo Experimental Forest, with data from Hall et al. 2013 [22, 50]. The reduction rate constant, k_{red} given by Calabrese and Porporato 2019 is $8.89 \times 10^{-15} \text{ kg}^2/\text{g}/\text{cells}/\text{d}$ and needs to be multiplied by the number of cells which ranges in their study from 1.0 to $2.5 \times 10^{11} \text{ cells}/\text{kg}$ [22]. This yields a range from about 0.0005 to $0.002 \text{ kg g}^{-1} \text{ d}^{-1}$. Values inferred from [108], [106], [104], and [3] agree with this range, but with a range of uncertainty coming from a lack of data on the electron donors. This study will place an upper bound on reduction rate at $k_r = 0.1 \text{ kg g}^{-1} \text{ d}^{-1}$ to account for the fact that in the model 10% or less of carbon may be available due to mineral protection, thus skewing the rate of reduction to be effectively lower. Oxidation rates, k_{ox} , also range over order of magnitudes. Stumm and Morgan 1992 report that at a pH of 5, $k_{ox} \approx 10 \times 10^{-6} \text{ s}^{-1}$ and at a pH of 7, $k_{ox} \approx 10 \times 10^{-2} \text{ s}^{-1}$ (864 d^{-1}), scaling with the concentration of hydroxide squared [116, 121]. A study by Ginn et al. 2017 found an oxidation rate in this range of 432 d^{-1} [22, 46]. Our concern is primarily with humid soils which are buffered by aluminum oxides at a pH of about 5.1, which will be taken as the approximate baseline [117]. In the base case of this model, it is assumed that sorption and desorption occur much faster than reduction, therefore k_s and k_d are assigned a value of 10 which assumes it is virtually instantaneous. The grams of carbon oxidized per gram of iron reduced, $\Omega = 0.054$, is found by assuming 4 moles of iron are reduced for each mole of carbon dioxide produced then converting units to grams [22, 124]. The ratio of mineral associated carbon to Fe^{3+} , ω , has been found by Zhao et al. 2017 to range from 0.56 to 17.7 molar ratio, or 0.12 to 3.80 mass ratio [145]. A value of $\omega = 2.87 \text{ gC}/\text{gFe}^{3+}$ was calculated from the ratio of released DOC to release

Parameter	Symbol	Value Range	Units
Reduction rate constant	k_{red}	(0.0005, 0.01)	kg/gC/d
Oxidation rate constant	k_{ox}	(0.086, 864)	d ⁻¹
C ox. to Fe ³⁺ red. ratio	Ω	0.054	
C to Fe ³⁺ association ratio	ω	(0.12, 3.80)	gC/gFe ³⁺
Aerobic decomp. rate constant	k_{aer}	(2.7×10^{-4} , 0.042)	d ⁻¹
Methanogenesis rate constant	k_{CH4}	$k_{aer}/10$	d ⁻¹
(De)sorption rate constant	k_s (k_d)	10	d ⁻¹

Table 3.1: Parameter ranges for the numerical model. See section 3.5.1 for sources.

Fe²⁺ in a study by Mikutta et al. 2024 [88]. The first order decay aerobic respiration constant used by Calabrese and Porporato 2019 is $k_{aer} = 2.74 \times 10^{-4} \text{ d}^{-1}$ and was taken from Bloomfield et al. 1993 [17, 22]. A survey of litterbag decomposition rates in rainforests by Powers et al. 2009 found a range of rates from 0.47 yr to 15.10 yr (0.00129 d^{-1} to 0.0414 d^{-1}) and that a single pool first order decomposition fit the data well [100]. Our model uses mineral protection and is modified by soil moisture, so the parameterization is not one to one, but these values give a good estimate of what aerobic decomposition rates may look like. All other anaerobic decomposition was lumped together into methanogenesis which is a complex multistep process usually involving a time lag [29, 86]. The rate of anaerobic decomposition (excluding via iron reduction) is slower than aerobic due to the lower Gibb’s free energy (ΔG) of the reaction [9, 12, 72]. In highly anoxic conditions there is a threshold beyond which decomposition is infeasible, which is around 16 kJ/mol C ΔG . Aerobic decomposition often has a $\Delta G \lesssim 100$ kJ/mol C [72]. Using a highly simplified thermodynamic argument, it is assumed here that anaerobic decomposition will occur about 10 times slower than the aerobic rate. This is generally reasonable as aerobic and anaerobic decomposition rates likely co-vary due to environmental factors such as temperature and microbial population.

Parameter	Symbol	Value	Units
Rooting Zone Depth	Z_r	0.4	m
Porosity	n	0.4	
Field Capacity	s_{fc}	0.8	
Stress Point	s^*	0.76	
Wilting Point	s_w	0.42	
Hydroscopic Point	s_h	0.36	
Evaporation Max	E_w	0.5	mm d ⁻¹
Transpiration Max	T_m	3.0	mm d ⁻¹

Table 3.2: Soil parameters used. Taken from Calabrese and Porporato 2019 [22] which obtained the data from Hall et al. 2013 [50].

3.5.2 Simulations

Several simulations were run with varying hydrological fluctuations forcing the system. The goal of the simulations is to understand the dynamics of the system under different hydrological fluctuations, parameter values, and initial conditions.

Static Soil Moisture

In the first set of simulations soil moisture is kept constant in anoxic conditions ($s = 1$). Under these conditions the impact of different concentrations of reactive Fe^{3+} is considered, ranging from 0 to 12 g/kg, with parameter values and initial carbon concentration kept constant. In the next simulation k_{red} was varied between 0.0005 and 0.0025 $\text{kg g}^{-1} \text{d}^{-1}$ with all else constant. In the third static soil moisture simulation ω was varied with all else constant between 0 and 4 gC/gFe^{3+} . The constant parameter values were $k_{red} = 0.0018 \text{ kg g}^{-1} \text{d}^{-1}$, $k_{ox} = 1 \text{ d}^{-1}$, $\omega = 3$, $k_{aer} = 0.002 \text{ d}^{-1}$, $\text{Fe}_0^{3+} = 6 \text{ g kg}^{-1}$, and $C_{i0} = 30 \text{ g}$.

Repeated Redox Cycles

In this section the effect of repeated redox cycles of a set length will be examined. This has been done in other simulations [21, 124] and experiments [46, 88]. The length

of redox cycles can vary from days in humid soils to weeks in wetlands and months in seasonally flooded soils or paddy fields [27]. The first simulation kept a constant cycle anoxic to oxic ratio of 5:1 with varying from 1 day anoxic 1/5 days oxic up to 80 days anoxic to 16 days oxic. The second simulation kept the length of the anoxic duration constant at 10 days and varied the length of the oxic duration from 1 day to 8 days. The parameter values are $k_{red} = 0.0018 \text{ kg g}^{-1} \text{ d}^{-1}$, $k_{ox} = 1 \text{ d}^{-1}$, $\omega = 3$, and $k_{aer} = 0.002 \text{ d}^{-1}$. The initial amounts of iron and carbon were varied for each run to have a low iron condition, $\text{Fe}_0^{3+} = 5 \text{ g kg}^{-1}$ and high iron condition $\text{Fe}_0^{3+} = 10 \text{ g kg}^{-1}$, and likewise a low carbon and high carbon condition $C_{i0} = 30 \text{ g kg}^{-1}$ and $C_{i0} = 60 \text{ g}$ respectively.

Stochastic Soil Moisture

In the third set of simulations soil moisture dynamics are included to imitate the dynamics of a soil in a humid climate where rainfall is frequent but random. There are two rainfall parameters. α , the mean depth of rainfall, is kept constant at a value of 12 mm. λ was varied between values of 0.5 d^{-1} and 1.5 d^{-1} . Parameters were kept at values of $k_{ox} = 0.1 \text{ d}^{-1}$, $k_{aer} = 0.002 \text{ d}^{-1}$, $k_{CH_4} = k_{aer}/10$. The parameter k_{red} was varied between 0.001 and 0.1, and the parameter ω was set to 0 for the no protection scenario and 3 gC/gFe^{3+} for the protection scenario.

3.6 Results

Here, the results of the simulations are presented. The unit used throughout to quantify the effect on emissions is total C loss which is the sum of carbon dioxide and methane emissions in grams of carbon per kilogram of soil.

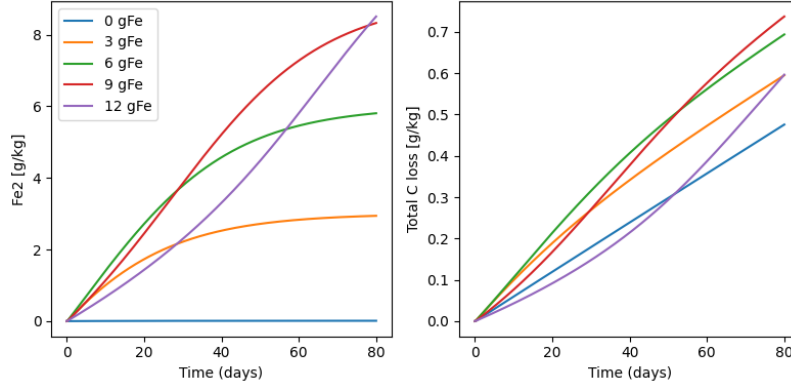


Figure 3.1: $k_{red} = 0.0018$, $k_{ox} = 1$, $k_{aer} = 0.002$, $s = 1$. The production of Fe^{2+} and carbon loss via mineralization (CO_2 production) is shown for several different initial iron concentrations under static anoxic conditions.

3.6.1 Results: Static Soil Moisture

The results for the simulations where soil moisture was kept constant at $s = 1$ are shown in table 3.3. Over an 80 day period, carbon loss increased with faster reduction rates, k_{red} , from 0.44 to 0.73 g/kg. Carbon loss decreased with higher protection rates (higher ω) but only slightly. The effect of initial iron concentrations are shown in the top row of table 3.3 and the entire dynamics are shown in figure 3.1. For no and low iron concentrations (0, 3, 6 g/kg) carbon loss increases with iron concentration as iron is used as the primary oxidant. However, as iron concentration increases to 9 and 12 g/kg, the initial carbon losses and iron reduction are low, but begin to increase quickly throughout the simulation. This second-order behavior is due to the fact that at the beginning a larger portion of the carbon is mineral associated and thus unavailable to decompose, but as iron is reduced the carbon is freed and it becomes available to be decomposed, leading to a feedback effect. As seen in the red line in figure 3.1 this feedback effect causes the slope to increase initially but is then limited by the concentration of iron in the system.

Table 3.3: Total Carbon loss in g/kg after 80 days of static anoxic conditions. Each top row shows the parameter varied (Fe_0^{3+} , k_{red} , ω) and each bottom row shows the corresponding C loss as carbon dioxide or methane.

Parameter Varied	Carbon Loss [g/kg]				
Fe_0^{3+} [g/kg]	0	3	6	9	12
C loss	0.48	0.60	0.69	0.74	0.60
k_{red} [kg/g/d]	0.0005	0.001	0.0015	0.002	0.0025
C loss	0.44	0.59	0.67	0.71	0.73
ω [gC/g Fe^{3+}]	0	0.5	1	2	4
C loss	0.79	0.78	0.77	0.76	0.76

Table 3.4: Total Carbon Loss after two years of redox cycles of set length. The ratio of all redox cycles is 5:1 anoxic:oxic, with anoxic periods of 1 day, 5 days, 20 days, and 80 days. Low iron and high iron is 5 g/kg and 10 g/kg respectively. Low carbon and high carbon is 30 g/kg and 60 g/kg respectively. Parameters used are described in section 3.5.2.

Ratio	1:1/5	5:1	20:4	80:16
Treatment	C Loss after 2 Years [g/kg]			
Low Fe + Low C	7.66	7.65	7.62	6.79
High Fe + Low C	4.19	4.24	4.35	5.44
Low Fe + High C	18.72	18.40	17.61	14.15
High Fe + High C	20.26	20.06	19.44	14.39

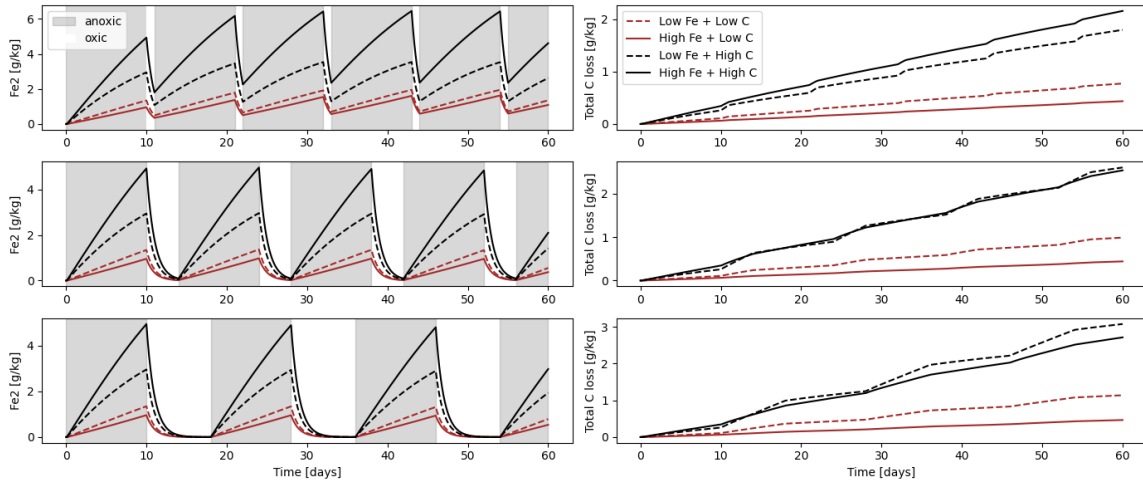


Figure 3.2: Simulations of redox cycles with different lengths of oxic periods are shown under high and low iron and high and low carbon conditions. Low Fe = 5 g/kg, High Fe = 10 g/kg, Low C = 30 g/kg, High C = 60 g/kg. Redox cycles of 10 d anoxic + 1 oxic, 10 d anoxic + 4 d oxic, and 10 d anoxic + 8 d oxic are shown. $k_{red} = 0.0018$, $k_{ox} = 1$, $k_{aer} = 0.002$.

3.6.2 Results: Redox Cycles

The total carbon loss after deterministic redox cycles with an anoxic:oxic ratio of 5:1 run for two years is shown in table 3.4. From this table it is evident that the longer redox cycles (20 and 80 days anoxic) had less carbon mineralization in all simulations except the high iron low carbon simulation, where they had more. This suggests that in all simulations except high Fe low C, iron reduction played a larger role than iron protection.

The redox cycles with a constant anoxic period (10 days) and varying length oxic period (1 day, 4 days, 8 days) is shown in figure 3.2. In the top row (1 day oxic) the high carbon high iron condition leads to the most decomposition. In the bottom row (8 days oxic) the low iron high carbon decomposes the most carbon. This switch between iron promoting versus hindering carbon decomposition is not seen in the low carbon simulations where low iron always leads to more decomposition. This suggests that only in the high carbon high scenario with much longer anoxic than oxic periods, iron's role as an oxidizer outweighs its role as a protector.

The results of this trial agree with those of Mikutta et al. 2024, which found that in successive redox cycles, higher carbon addition leads to greater iron reduction [88]. Chen et al. 2020 found that in oxic conditions, when carbon and iron are added to a soil together, iron will protect the carbon and lead to lower emissions, but can lead to higher CO₂ emissions under fluctuating conditions [23].

3.6.3 Results: Stochastic Soil Moisture

The results of two simulations run for year with stochastic rainfall are shown in figure 3.3. In the first simulation (top row) $\alpha = 12\text{mm}$ is the mean depth of rainfall and $\lambda = 0.5\text{d}^{-1}$ is the mean frequency of rainfall, i.e. it rains on average once every two days (very wet climate). In the second simulation (bottom row) α is the same,

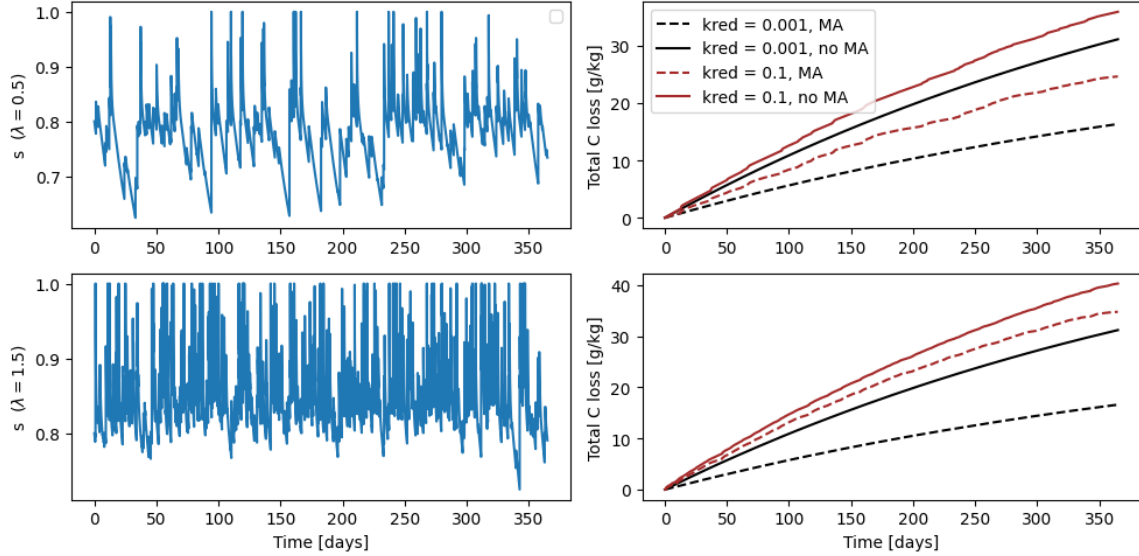


Figure 3.3: Simulations of soil moisture under stochastic rainfall. The parameter k_{red} was evaluated at a value of $0.001 \text{ kg g}^{-1} \text{ d}^{-1}$ and $0.1 \text{ kg g}^{-1} \text{ d}^{-1}$. The protection case (MA) had $\omega = 3$ and the no-protection case (no MA) had $\omega = 0$. The other parameter values used are described in section 3.5.2.

but $\lambda = 1.5 \text{ d}^{-1}$, i.e. it rains more than once day on average. The wet simulation is meant to imitate to the conditions seen in a lowland or wetland where water table fluctuations and rainfall both contribute to a situation where anoxic conditions are dominant but still random. Both simulations were run with slow reduction, $k_{red} = 0.001 \text{ kg g}^{-1} \text{ d}^{-1}$, or fast reduction, $k_{red} = 0.1 \text{ kg g}^{-1} \text{ d}^{-1}$ and no protection (no MA) where $\omega = 0$ and protection (MA) where $\omega = 3$. In the less rainy scenario no protection leads to higher decomposition in both cases. On the other hand in the rainy scenario higher reduction with mineral protection leads to faster decomposition than no mineral protection and slow reduction. This shift demonstrates that under certain hydrological conditions the dominant mechanism of carbon decomposition can change.

3.7 Discussion

The results demonstrate the wide array of effects of iron on carbon decomposition depending on the redox cycles, initial conditions, and parameter values such as reduction rate, oxidation rate, and carbon to iron attachment ratio. First, the initial iron concentration can have a major impact on the redox dynamics. In the static flooded simulation it was shown that when iron levels are high enough there will be a feedback effect wherein iron reduction will free carbon and lead to faster iron reduction (figure 3.1). This is important to note as it demonstrates that duration of the anoxic period plays an important role in the dynamics. Most experiments are run with redox cycles of days to weeks [23, 46, 88, 108], however having a redox cycle of only twenty days would yield results that show that higher iron leads to less CO₂ (due to protection) and extending the experiment would show the opposite. This is what is demonstrated in Huang and Hall 2017 [58] in an experiment where soils were kept at field capacity or saturated for an extended period. After 25 days, the field capacity soils (oxic) had higher cumulative CO₂ emissions, as expected due to the high redox potential of oxygen. However after that the rate of CO₂ and CH₄ emissions increased in the saturated soil, leading to higher carbon emissions in the saturated soil after about 30 to 40 days [58]. This highlights the criticality of time scales in the dynamics of iron and carbon cycles and suggest that results from short term experiments may not capture the correct direction in the long term due to the release of protected carbon. Our simulation also points to the importance of understanding how large the reactive iron pool is (primarily poorly crystalline short range order iron oxides), as much of the iron in soils is stable and will not be reduced, except perhaps in the case of large scale leaching of iron [106].

The results from the redox cycles (table 3.4 and figure 3.2) demonstrate the importance of both the ratio of anoxic to oxic and the timescale of the fluctuation. In

table 3.4 it is evident that longer cycles (80:16) lead to lower mineralization of carbon in all conditions except high iron low carbon. This is because in that case the longer period of reduction allowed most of the carbon to become free and available for reduction which was not the case under shorter redox cycles. Under the high carbon cases, the longer redox cycles significantly decreased the total carbon mineralization (29% lower than 1:1/5 day cycles), likely due to iron limitations. When redox cycles reach a certain length, all of the reactive iron is reduced and is no longer available as an oxidizer and thus less energetically favourable and slower reactions like methanogenesis dominate decomposition [2, 85, 124]. In the second simulation, where the anoxic length is set at 10 days and oxic length varies (figure 3.2) there are shifting relationships between carbon mineralization, initial iron, and initial carbon concentration. Under low carbon conditions low iron always lead to more decomposition regardless of the redox cycle, suggesting that mineral protection dominated and reduced mineralization. Under high C greater iron lead to more decomposition when anoxic conditions dominated. These results agree with a study by LaCroix et al. 2019 [70] which found a high correlation between reducible Fe and carbon stores in upland soils (mostly oxic conditions), but no correlation in lowland, seasonally flooded soils which experience long durations of anoxic conditions.

In the third set of simulations stochastic rainfall was considered for a wet soil ($\lambda = 0.5 \text{ d}^{-1}$) and very wet soil ($\lambda = 1.5 \text{ d}^{-1}$) and is shown in figure 3.3. The two major controls on carbon mineralization by iron are iron reduction which depends on k_{red} and the role of iron as a protector of carbon, which depends on the carbon to iron mineral association ratio, ω . We see that in the less wet soil the effect of mineral association is a more important than k_{red} . This relationship changes in the very wet soil as more carbon is mineralized under the higher reduction rate with mineral protection than a low reduction rate without mineral protection. These results also compare and contrast the dynamics of a soil while including mineral protection and

without including it. When mineral protection is not included there is significantly more decomposition in both scenarios, and the difference between high reduction and low reduction is smaller. When mineral association is included, the rate of reduction becomes critical because it plays a two-fold role in the rate that carbon is oxidized and the rate that it loses protection. The stochasticity of the rainfall appears to be “smoothed” by the slower rates of reduction and decomposition. Most soils in humid climates are closer to the less wet scenario. The implications of this are that mineral protection, even in a relatively wet climate can be significant relative to the role of iron as an oxidant.

Overall, this simple numerical model that captures key relations between iron, carbon, and hydrology demonstrates a wide range of behavior. Most surprising was the model’s dependence on the initial conditions of the amount of reactive iron and carbon in the soil. The maximum protective capacity of the iron in this model is equal to $\text{Fe}^{3+}\omega$. In the case where carbon exceeds this value there is ample free carbon to decompose. In the case where carbon is equal to or less than this value only a small fraction of the carbon at any time is available to decomposition and thus the dynamics are highly dependent on the rate of reduction of iron, with a non-linear feedback loop leading to an acceleration of iron reduction and carbon decomposition in anoxic conditions. This acceleration is demonstrated in our figure 3.1 and aligns with the observations of Huang and Hall 2017 [58], although more work is needed to verify this acceleration/feedback effect. The two effects, protection and reduction, already demonstrate a variety of dynamics, yet they alone do not capture the entire picture of the coupled iron carbon cycles. A few of the components not included are microbes, pH levels, Fenton reactions, iron leaching, co-precipitation, crystallization, photosynthetic reactions, and plant interactions [23, 28, 36, 51, 106, 118, 124]. Another drawback of this model is that despite its simplicity, it is not available to analytical analysis under fluctuating redox conditions. An analytical

analysis of the stochastic model is performed in the chapter 4 to find functional relationships between hydrological variables and iron reduction.

Chapter 4

Analytical Solution to the Stochastic Ferrous Wheel

4.1 Problem Formulation

To intuitively understand a system, it is of major benefit to have an analytical solution wherein the relation between key variables is clear and interpretable. Unfortunately, most environmental systems are described by non-linear dynamical models which can not be solved analytically, as is the case with the model developed in chapter 3. It is occasionally possible, however, to simplify the system by making assumptions in order to obtain analytical solutions. This is the case for instance for groundwater flow around a well or the equations of the Ekman spiral in atmospheric and ocean flows [40, 44]. Here, a novel analytical solution is derived from a simplified model of the soil iron cycle for the case of stochastic fluctuations between oxic and anoxic conditions. This solution is then used to derive analytical functions of hydrological variables and iron cycle parameters to predict trends in carbon oxidation and protection. The purpose of this is to gain an understanding behind the dynamics of the soil iron cycle in different climates that is not possible from numerical models. Understanding the

soil iron cycle will then directly lead to an improved understanding of the carbon cycle due to their coupling.

Just as the previous section built on a numerical model developed by Calabrese and Porporato 2019, this section will build on the simplified, analytic model of the iron cycle of Calabrese et al. 2020 [21, 22]. The first simplification is to reduce the model to its two most important components, reduction and oxidation. This assumes that there is a roughly constant reactive iron pool (Fe^{tot}) that can be in its oxidized state (Fe^{3+}) or reduced state (Fe^{2+}). The approximation of a constant reactive iron pool is discussed further in Appendix 6.1.

The simplified system can be written using two compartment equations as

$$\frac{d\text{Fe}^{2+}}{dt} = \text{RED}(\text{Fe}^{3+}) - \text{OX}(\text{Fe}^{2+}) \quad (4.1)$$

and

$$\frac{d\text{Fe}^{3+}}{dt} = -\text{RED}(\text{Fe}^{3+}) + \text{OX}(\text{Fe}^{2+}). \quad (4.2)$$

In equations (4.1) and (4.2) the RED and OX terms represent the same as in equations (3.7) and (3.8), but will be formulated differently here.

It is now assumed that soil organic carbon and iron reducing microbes are constant, such that reduction becomes a first order reaction only dependent on Fe^{3+} and redox potential of the soil. Redox conditions are represented by a term, $\xi(t)$, yielding reduction and oxidation equations of

$$\text{RED} = k_r \text{Fe}^{3+} \xi(t), \quad \text{OX} = k_o \text{Fe}^{2+} (1 - \xi(t)). \quad (4.3)$$

Here, $k_o = k_{ox}$ as used in equation (3.9). However the reduction constant, k_r , does not equal k_{red} as used in (3.10). Instead, equation (4.3) treats reduction as a first-order process dependent only on Fe^{3+} and thus k_r has unit of 1/day. This makes it

an implicit approximation $k_r \approx k_{red} \overline{C}_l$ where \overline{C}_l is the average available carbon.

When conditions are anoxic $\xi(t)$ approaches zero, while in oxic conditions it is almost one. Since total iron (Fe^{tot}) is conserved Fe^{3+} can be written in terms of Fe^{2+}

$$\text{Fe}^{\text{tot}} = \text{Fe}^{2+} + \text{Fe}^{3+} \rightarrow \text{Fe}^{3+} = \text{Fe}^{\text{tot}} - \text{Fe}^{2+}, \quad (4.4)$$

where Fe^{tot} is a constant. Now, the system of two equations is reduced to just a single equation for Fe^{2+} . The equation can be normalized by dividing by Fe^{tot} to yield a new state variable, $x = \frac{\text{Fe}^{2+}}{\text{Fe}^{\text{tot}}} \in [0, 1]$. Combining equations (4.1), (4.4), and (4.3) and substituting in for x yields

$$\frac{dx}{dt} = k_r(1 - x)\xi(t) - k_o x(1 - \xi(t)). \quad (4.5)$$

This equation describes the evolution of the fraction of Fe^{2+} in the soil driven by soil moisture fluctuations in the $\xi(t)$ term. k_r contains within it the various factors influencing reduction rate, such as mineral properties, available surface area, presence of electron donors, and population of iron reducers (see section 2.2.1) [21, 34, 106].

The term $\xi(t)$ represents the redox state of the soil, which is primarily driven by the abundance of O_2 . The oxygen content in the soil is a highly non-linear function of soil moisture, remaining near saturation from $s = 0$ up until field capacity, then rapidly increasing to anoxic conditions near saturation [50, 115]. To simplify the system, the soil is divided into two states, oxic when s is less than some threshold value, and anoxic when s exceeds the threshold, following Calabrese et al. 2020 [21]. The redox term is then assigned to be binary: $\xi(t) = 0$ in oxic conditions and $\xi(t) = 1$ in anoxic conditions [21]. The system is now driven by stochastic switches between redox states. It is assumed that $\xi(t)$ changes in time following a Dichotomous Markov process where it switches from oxic to anoxic ($\xi(t) = 0 \rightarrow 1$) with a rate k_1 and switches from anoxic to oxic ($\xi(t) = 1 \rightarrow 0$) with rate k_2 . Both rates are determined

by the stochastic soil moisture dynamics [102].

There are two possible ways to represent the system mathematically. The first method is called the functional representation and it frames equation (4.5) as a stochastic differential equation (SDE) as follows [102]

$$\frac{dx}{dt} = f(x) + g(x)\xi(t) = -k_o x + [k_r(1-x) + k_o x] \xi(t). \quad (4.6)$$

The second representation, called the mechanistic approach, poses the dynamics as a piece-wise equation. If conditions are oxic the change in x is driven by one function, $f_o(x) = -k_o x$, and if conditions are anoxic it is governed by another function, $f_a(x) = k_r(1-x)$ [102]

$$\frac{dx}{dt} = \left\{ \begin{array}{ll} -k_o x, & s \leq s_{crit} \quad (\xi(t) = 0) \\ k_r(1-x), & s > s_{crit} \quad (\xi(t) = 1) \end{array} \right\}. \quad (4.7)$$

If a switch from anoxic to oxic occurs at time t_0 with $x(t_0) = x_0$, the dynamics until the next switch can be solved as a simple exponential ODE to yield

$$x(t) = x_0 e^{-k_o(t-t_0)}. \quad (4.8)$$

Similarly the deterministic dynamics when conditions switch from oxic to anoxic can be solved to find

$$x(t) = 1 - (1 - x_0)e^{-k_r(t-t_0)}. \quad (4.9)$$

4.2 Deriving the Steady State Probability Density Function

Now that the problem is mathematically defined, the steady-state solution under stochastic redox fluctuations can be found. The steady-state PDF is a function with

area of unity that describes the theoretical probability of finding the state variable (x) in a particular infinitesimal range, dx . Let $p(x, 0; t)dx$ represent the probability of the state variable being x while $\xi(t) = 0$ (oxic conditions) at time t . Beginning from the Chapman-Kolmogorov equation, the forward Kolmogorov equation can be derived as done in Ridolfi et al. 2007 [102]. The forward Kolmogorov equation describes the change in the probability of being at a state (x, ξ, t) in time and can be written for $\xi = 0$ as follows (ξ is used in place of $\xi(t)$ for notations sake),

$$\frac{\partial p(x, 0, t)}{\partial t} = -\frac{\partial}{\partial x} [p(x, 0, t)f_o(x)] - p(x, 0, t)k_1 + p(x, 1, t)k_2. \quad (4.10)$$

Where the change in probability of being in state $\xi = 0$ is positively correlated with the rate of switching from state $\xi = 1$ to state $\xi = 0$ (k_2) and negatively correlated with the rate of switching from state $\xi = 0$ to state $\xi = 1$ (k_1) as expected. The same procedure is followed to write the forward Kolmogorov for being at $(x, 1, t)$ as

$$\frac{\partial p(x, 1, t)}{\partial t} = -\frac{\partial}{\partial x} [p(x, 1, t)f_r(x)] - p(x, 1, t)k_2 + p(x, 0, t)k_1. \quad (4.11)$$

The steady-state PDFs of these equations can be found by setting the time derivatives to 0 and integrating with respect to x .

$$p(x, 0) = \frac{C}{f_o(x)} \exp \left\{ -\int_x \frac{k_1}{f_o(x')} + \frac{k_2}{f_r(x')} dx' \right\} \quad (4.12)$$

$$p(x, 1) = -\frac{C}{f_r(x)} \exp \left\{ -\int_x \frac{k_1}{f_o(x')} + \frac{k_2}{f_r(x')} dx' \right\}. \quad (4.13)$$

In these equations C is an integration constant that is determined so that the marginal distribution of x integrates to unity. The marginal distribution of x , $p_X(x)$ can be found by summing over the possible states of ξ : $p_X(x) = p(x, 0) + p(x, 1)$. Written

out it becomes [102]

$$p_X(x) = C \left[\frac{1}{f_o(x)} - \frac{1}{f_r(x)} \right] \exp \left\{ - \int_x \frac{k_1}{f_o(x')} + \frac{k_2}{f_r(x')} dx' \right\}. \quad (4.14)$$

Solving this equation for the system yields

$$p_X(x) = \frac{C}{k_o} \left[1 + x \left(\frac{k_o}{k_r} - 1 \right) \right] x^{\frac{k_1}{k_o} - 1} (1 - x)^{\frac{k_2}{k_r} - 1}. \quad (4.15)$$

This distribution reduces to the well studied beta distribution when $k_o = k_r$ [1, 61]. Buckingham Pi Theorem states that given n variables and m fundamental dimensions, $n - m$ dimensionless groups can be formed which provide fundamental relations [20]. In this system there are $n = 4$ free variables and $m = 1$ dimension, time. Therefore, there should be three dimensionless variables that can describe the system. Here, the PDF cleanly defines three dimensionless ratios, $\phi = \frac{k_1}{k_o}$, $\theta = \frac{k_2}{k_r}$, and $\beta = \frac{k_o}{k_r}$. The PDF can be re-written as

$$p_X(x) = C_x [1 + x(\beta - 1)] x^{\phi - 1} (1 - x)^{\theta - 1}. \quad (4.16)$$

Where $C_x = \frac{C}{k_o}$ is found by setting the integral of the PDF from 0 to 1 equal to one and solving. C_x has the following analytic form

$$C_x = \left[B(\phi, \theta) \left[1 + (\beta - 1) \frac{\phi}{\phi + \theta} \right] \right]^{-1}. \quad (4.17)$$

Where $B(\phi, \theta)$ is the beta function given by

$$B(\phi, \theta) = \frac{\Gamma(\phi)\Gamma(\theta)}{\Gamma(\phi + \theta)}, \quad (4.18)$$

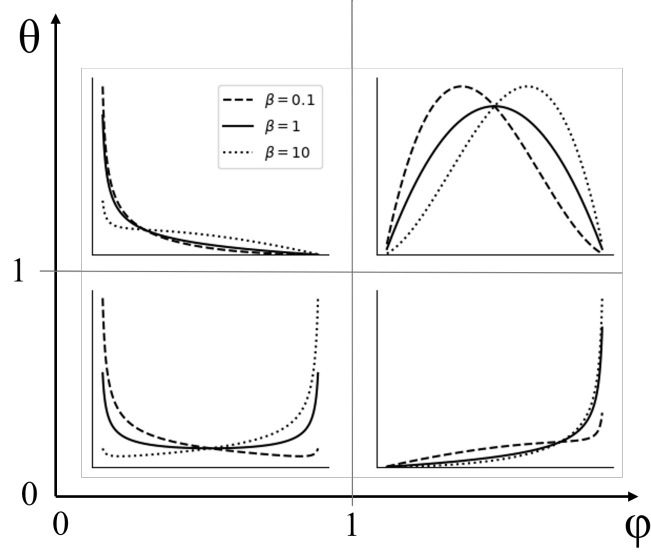


Figure 4.1: PDF of x for different values of ϕ , θ , and β . The plot is split by critical points ($\theta = 1$ and $\phi = 1$). The subgraphs plot x on the x-axis from 0 to 1 against $p_X(x)$ on the y-axis.

where $\Gamma(x)$ is the gamma function, which is just the factorial if x is a natural number.

The cumulative distribution function (CDF) is defined generally as

$$P_X(x) = \int_0^x p_X(x') dx'. \quad (4.19)$$

In this case it can be solved to yield

$$P_X(x) = \frac{C_x}{B(\phi, \theta)} \left[B_x(\phi, \theta) + (\beta - 1) \left(B_x(\phi, \theta) - \frac{x^\phi (1-x)^\theta}{\phi} \right) \right], \quad (4.20)$$

where C_x is defined in equation (4.17). $B_x(\phi, \theta)$ is the incomplete beta function defined as

$$B_y(\phi, \theta) = \int_0^y x^{\phi-1} (1-x)^{\theta-1} dx. \quad (4.21)$$

4.2.1 Mean

The expectation of x can be found by integrating the PDF multiplied by x as follows

$$\mathbf{E}(x) = C_x \int_0^1 x [1 + x(\beta - 1)] x^{\phi-1} (1-x)^{\theta-1}. \quad (4.22)$$

This has the solution

$$\mathbf{E}(x) = \frac{\phi}{\phi + \theta} \frac{1 + (\beta - 1) \frac{\phi+1}{\phi+\theta+1}}{1 + (\beta - 1) \frac{\phi}{\phi+\theta}}. \quad (4.23)$$

As a sanity check for equation (4.23), the expectation correctly reduces to the mean of a beta distribution: $\phi/(\phi + \theta)$ for $\beta = 1$ ($k_o = k_r$) [61]. This derivation relates four parameters (k_o, k_r, k_1, k_2), oxidation rate, reduction rate, transition rate to anoxic conditions, and transition rate to oxic conditions respectively to the average fraction of active iron that is ferrous. This fraction has important ramifications for iron availability, iron leaching, and the interactions of iron with the carbon cycle. The moment generating function of the PDF can be found analytically, allowing one to derive any higher moment (e.g. variance), however it is an unwieldy equation that is not shown here.

4.2.2 Crossing Times

The frequency of crossing a certain threshold can be an important variable to know for many environmental variables. For instance the amount of time under stress from lack of water or a nutrient can be determined from level-crossing statistics [99]. The frequency of crossing a level ε can be given by the following general formula [99, 129],

$$v(\varepsilon) = \int |\dot{x}| p(\varepsilon, \dot{x}) d\dot{x}. \quad (4.24)$$

Where \dot{x} is the rate of change of x . For stationary conditions, the frequency of upcrossing must equal the frequency of downcrossings ($v(\varepsilon) = v^\uparrow(\varepsilon) = v^\downarrow(\varepsilon)$) [99]. When the loss or gain functions of the state variable are known, the crossing frequency can be intuitively derived as follows (following Porporato and Yin 2022) [98, 99]. By definition the fraction of time a variable is in an interval $\varepsilon + d\varepsilon$ is given by $p(\varepsilon)d\varepsilon$. The fraction of time a variable is in the same interval is also equal to the frequency of crossing the interval, $v(\varepsilon)$, times the amount of time spent it takes to cross the interval, assuming there are no switches while crossing. The time it takes to cross the interval is $d\varepsilon/|\rho^{\uparrow(\downarrow)}(\varepsilon)|$, where $\rho^{\uparrow(\downarrow)}(\varepsilon)$ is the slope of the variable at the upcrossing (downcrossing). Because $p(\varepsilon)d\varepsilon$ and the frequency times the time it takes to cross the interval both represent the fraction of time spent in the interval, it can be written that

$$p(\varepsilon)d\varepsilon = v(\varepsilon)\frac{d\varepsilon}{|\rho^\uparrow(\varepsilon)|} + v(\varepsilon)\frac{d\varepsilon}{|\rho^\downarrow(\varepsilon)|} = v(\varepsilon)d\varepsilon\left(\frac{1}{|\rho^\uparrow(\varepsilon)|} + \frac{1}{|\rho^\downarrow(\varepsilon)|}\right). \quad (4.25)$$

Solving for $v(\varepsilon)$ yields,

$$v(\varepsilon) = p(\varepsilon)\frac{|\rho^\uparrow(\varepsilon)\rho^\downarrow(\varepsilon)|}{|\rho^\uparrow(\varepsilon)| + |\rho^\downarrow(\varepsilon)|}. \quad (4.26)$$

It is known that $\rho^\uparrow(\varepsilon) = (1 - \varepsilon)k_r$, $\rho^\downarrow(\varepsilon) = -k_o\varepsilon$, and $p(\varepsilon)$ from equation (4.15).

Substituting yields

$$v(\varepsilon) = Ck_o\varepsilon^\phi(1 - \varepsilon)^\theta. \quad (4.27)$$

From here, the mean duration of an excursion below a threshold, $\bar{T}_\varepsilon^\downarrow$, can be derived.

The fraction of time spent below ε by definition is the CDF at ε , $P(\varepsilon)$. It is also equal to the mean duration of an excursion times the frequency of excursion, $\bar{T}_\varepsilon^\downarrow v(\varepsilon)$.

Solving for the average duration gives

$$\bar{T}_\varepsilon^\downarrow = \frac{P(\varepsilon)}{v(\varepsilon)}. \quad (4.28)$$

Similarly, the mean time above can be derived to yield

$$\bar{T}_\varepsilon^\uparrow = \frac{1 - P(\varepsilon)}{v(\varepsilon)} = \frac{1}{v(\varepsilon)} - \bar{T}_\varepsilon^\downarrow. \quad (4.29)$$

Combining equations (4.20), (4.27), and (4.28) gives an expression for the average duration of an excursion below a threshold in terms of the three dimensionless parameters. Substituting in equations (4.27) and (4.20) into equations (4.28) and (4.29) is left as an exercise for the reader.

4.3 A simplified Soil Moisture Model

In $p_X(x)$ (equation (4.16)) there is a dependency on k_1 and k_2 , the average frequency at which conditions switch from oxic to anoxic and from anoxic to oxic respectively. These parameters depend on the hydrology of the soil, as conditions are assumed to be anoxic when $s > s_c$ and oxic when $s \leq s_c$. Due to the randomness of rainfall, s is itself a random variable driven by an SDE. If the dynamics of s are known, then k_1 and k_2 can be derived, connecting the PDF of iron to the hydrological parameters of the system. The frequency of switching from oxic to anoxic conditions, k_1 , is equal to the reciprocal of the average length of excursion below s_c , $\bar{T}_{s_c}^\downarrow$. This is also the average duration that oxic conditions persist and so for neatness $\bar{T}_{s_c}^\downarrow = \tau_o$. Similarly, $k_2 = 1/\tau_a$, where τ_a is the average duration that anoxic conditions persist.

The iron system was solved assuming that the switches between oxic and anoxic are dichotomous Markov noise (DMN). If this were the case, the distribution of the lengths of excursions would be exponential with mean τ_o and τ_a . In reality, the memory of the soil moisture means that the process is not Markovian and the lengths of excursions are not exactly exponentially distributed. Here, by assuming DMN, the approximation is made that the distribution of excursions is exponential. This assumption is reviewed in section 6.2.

For the numerical model, the dynamics for s , given by equation (3.1), included non-linear losses from leakage ($L(s)$) and a piece-wise loss function for evapotranspiration ($ET(s)$). Rodriguez-Iturbe et al. 1999 derived the complete steady-state PDF of this equation, but it is piece-wise and difficult to interpret [109]. A minimalist model proposed by Porporato et al. 2004 provides a good approximation of the complete model, but has a much simpler steady-state PDF [98]. This model will now be explained and the PDF derived.

First, an effective relative soil moisture, y , is defined that ranges between s_w and s_l [98, 99]. It is assumed that due to rapid leakage at $s > s_l$, the losses are infinite and thus y can not exceed s_l . Similarly, losses approach 0 at s_w and thus y can not descend below wilting point. Mathematically, y is represented as

$$y = \frac{s - s_w}{s_l - s_w} \quad (4.30)$$

such that at $s = s_w$, $y = 0$ and at $s = s_l$, $y = 1$, where s_l is some soil moisture between field capacity (s_{fc}) and saturation ($s = 1$) [98, 99]. The new storage capacity of the soil is defined as $w_0 = nZ_r(s_l - s_w)$ [98, 99]. When rainfall exceeds this storage capacity it is assumed to runoff and/or leak out immediately. The system is governed by the state equation

$$\frac{dy}{dt} = I - E(y), \quad (4.31)$$

where I is a jump process representing impulses of rain and $E(y)$ are the losses from evapotranspiration and leakage. Cumulative losses in the range of effective soil moisture are assumed to be a linear function of y defined as

$$E(y) = \eta y. \quad (4.32)$$

Where $\eta = ET_{max}/w_0$ is the normalized evapotranspiration. As in section 3.1.1, α

is the mean depth of rainfall which is exponentially distributed. Similarly, λ is the frequency of rainfall, where time between rainfalls is exponentially distributed. A new dimensionless parameter, $\gamma = w_0/\alpha$, is defined as the inverse of normalized rainfall depth. With these parameters the PDF of y can be solved for using a Kolmogorav master equation with jumps [98, 99] to yield

$$p_Y(y) = \frac{C_y}{\eta} e^{-\gamma y} y^{\frac{\lambda}{\eta}-1}. \quad (4.33)$$

Where C_y is an integration constant such that the PDF integrates to unity. The cumulative distribution function can be found by integrating $p_Y(y)$ from 0 to y to yield

$$P_Y(y) = \frac{C_y}{\eta} \frac{\Gamma(\frac{\lambda}{\eta}) - \Gamma(\frac{\lambda}{\eta}, \gamma y)}{\gamma^{\frac{\lambda}{\eta}}}. \quad (4.34)$$

Now, the level crossing statistics (frequency and average duration) can be calculated in the same way as was done for x in section 4.2.2. The dynamics of soil moisture differ from x because x was forced with DMN, but y is forced with white shot noise [99]. Because y only increases via these random pulses of rainfall that are assumed to be instantaneous, the rate of upcrossing a threshold ε approaches infinity in the model. Therefore equation 4.26 reduces to

$$v_Y(\varepsilon) = p_Y(\varepsilon) |E(\varepsilon)| \quad (4.35)$$

where $\rho(\varepsilon) = E(\varepsilon)$ is still the slope of the state equation at ε . The threshold of interest is the oxic/anoxic transition, s_c . In terms of effective soil moisture the equivalent y_c can be found using equation (4.30). From here, the general equation (4.28) can be combined with the equations for y , (4.33), (4.34) and (4.35), to find the average

duration of oxic conditions, τ_o . The equation for τ_o is

$$\tau_o = \frac{\Gamma(\frac{\lambda}{\eta}) - \Gamma(\frac{\lambda}{\eta}, \gamma y_c)}{\gamma^{\frac{\lambda}{\eta}} e^{-\gamma y_c} y_c^{\frac{\lambda}{\eta}} \eta}. \quad (4.36)$$

The average frequency of transitioning from oxic to anoxic (k_1) can be written as

$$k_1 = \frac{1}{\tau_o} = \frac{\gamma^{\frac{\lambda}{\eta}} e^{-\gamma y_c} y_c^{\frac{\lambda}{\eta}} \eta}{\Gamma(\frac{\lambda}{\eta}) - \Gamma(\frac{\lambda}{\eta}, \gamma y_c)}. \quad (4.37)$$

Similarly, the average frequency of transitioning from anoxic to oxic can be found using equation (4.29) to be

$$k_2 = \frac{C_y \gamma^{\frac{\lambda}{\eta}} e^{\gamma y_c} y_c^{\frac{\lambda}{\eta}}}{\gamma^{\frac{\lambda}{\eta}} - (\Gamma(\frac{\lambda}{\eta}) - \Gamma(\frac{\lambda}{\eta}, \gamma y_c))}. \quad (4.38)$$

The average total length of a redox cycle is the sum of the average length of excursion below and above the oxic threshold, given by $T = \tau_o + \tau_a$. The total fraction of time spent in anoxic conditions, f , is given by the ratio $f = \tau_a/T$, or the complementary CDF $f = 1 - P_Y(y_c)$ (equation (4.34)).

4.4 Quantifying Total Reduction

One of the motivations behind studying the iron cycle is to determine its role in carbon decomposition and thus green house gas emissions. Ferric iron (Fe^{3+}) is one of the most important electron acceptors when oxygen is not available, and as such it contributes greatly to the decomposition of organic matter under anoxic conditions [2, 51, 121]. A natural assumption is that the greater the prevalence of anoxic conditions, the more iron is reduced in the decomposition of SOM. However, as explored in Calabrese et al. 2020, the total iron reduction depends not only on the fraction of time in anoxic conditions, but also the length of the redox cycles [21]. As anoxic conditions

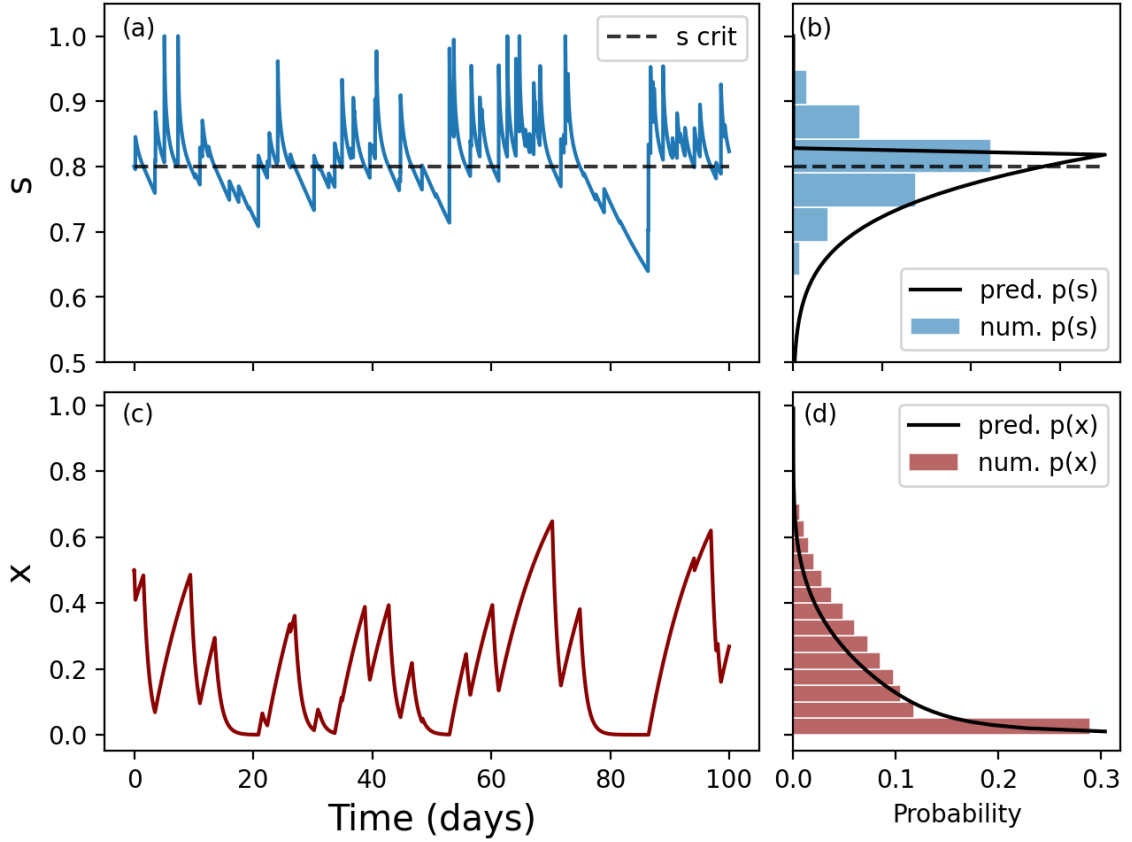


Figure 4.2: (a) shows the complete dynamics of s described in section 3.1 with parameters $\alpha = 12 \text{ mm}$ and $\lambda = 0.82 \text{ d}^{-1}$ over a 100 day run. In (b) the shaded region shows the normalized histogram of s after 10,000 days of simulation which approximates the numerically derived steady-state PDF. The black line in (b) is the PDF of s derived from the simplified soil moisture model using equation 4.33 with the same parameters. (c) shows the numerical dynamics of $x = \text{Fe}^{2+}/\text{Fe}^{\text{tot}}$ driven by the soil moisture in (a) with $k_o = 1$ and $k_r = 0.1 \text{ d}^{-1}$. The shaded region in (d) shows the normalized histogram after 10,000 days and the black line shows the PDF prediction based off the simplified model and simplified soil moisture model (equation (4.15)).

persist, the available Fe^{3+} is used up and no longer available as an oxidant. Upon switching to oxic conditions iron is rapidly oxidized, regenerating the pool of Fe^{3+} that can be used in the next anoxic cycle [21]. In the 2020 paper, Calabrese et al. explore the effects of constant length redox cycles on average rates of reduction. Here, this is expanded to the stochastic case by assuming fluctuations follow DMN. The objective of this section is to find the distribution and expected value of reduction rates using the results from the PDF of x . In the simplified iron system, reduction is approximated as a first order process using equation (4.3), rewritten here for convenience.

$$\text{RED} = k_r \text{Fe}^{3+} \xi(t) = k_r \text{Fe}^{\text{tot}} \xi(t) (1 - x). \quad (4.39)$$

Where $\text{Fe}^{\text{tot}} = \text{Fe}^{2+} + \text{Fe}^{3+}$ is a constant, and $\xi(t)$ is a random variable that is equal to 1 in anoxic conditions and 0 in oxic conditions. Both sides of equation (4.39) are divided by Fe^{tot} and k_r to get a normalized, dimensionless reduction rate, r :

$$r = \frac{\text{RED}}{\text{Fe}^{\text{tot}} k_r} = (1 - x) \xi(t). \quad (4.40)$$

Conditioned on $\xi = 1$, the conditional distribution of r can be written

$$p_R(r|\xi = 1) = p_X(1 - x|\xi = 1) = \frac{p_X(1 - x, \xi = 1)}{p(\xi = 1)} = \frac{p_R(r, \xi = 1)}{p(\xi = 1)}. \quad (4.41)$$

Where the third and fourth equalities come from the definition of a conditional distribution. The joint distribution $p(x, 1)$ can be directly derived from equation (4.13) to yield

$$p(x, 1) = \frac{C}{k_r} x^\phi (1 - x)^{\theta-1}. \quad (4.42)$$

Where $C = C_x k_o$ has a dimension of 1/time and can be found from (4.17). The integration constants take on importance when dealing with joint and marginal distributions because in a joint distribution integrating over the domain of just one

variable will not integrate to one, one must integrate over both variables. The constant C will be replaced with a new dimensionless constant of integration C_r such that

$$C_r = \frac{C}{k_r} = C_x \frac{k_o}{k_r} = \frac{\beta}{B(\phi, \theta) \left[1 + (\beta - 1) \frac{\phi}{\phi + \theta} \right]}. \quad (4.43)$$

The marginal distribution of r can be found by simply substituting in $r = 1 - x$ into equation (4.42) to obtain

$$p(r, 1) = C_r (1 - r)^\phi r^{\theta-1}. \quad (4.44)$$

Integrating r from 0 to 1 will yield the marginal distribution of $\xi = 1$ which is just the fraction of time that the system is in anoxic conditions. The joint distribution when $\xi = 0$ is given by

$$p(r, 0) = (1 - f)\delta(r). \quad (4.45)$$

Where $\delta(r)$ is the Dirac delta or unit impulse function which is equal to one when $r = 0$ and zero otherwise. Summing the joint probability distributions the marginal PDF of r can be found to be

$$p_R(r) = (1 - f)\delta(r) + C_r (1 - r)^\phi r^{\theta-1}. \quad (4.46)$$

Substituting in for f and C (equation (4.17)), yields

$$p_R(r) = \frac{k_2}{k_1 + k_2} \delta(r) + \frac{\beta(1 - r)^\phi r^{\theta-1}}{B(\phi, \theta) \left[1 + (\beta - 1) \frac{\phi}{\phi + \theta} \right]}. \quad (4.47)$$

The first term in (4.47) is the fraction of time in oxic conditions times an impulse function at $r = 0$ and represents the fact that reduction is zero in oxic conditions. The second term is a beta distribution with an area underneath equal to $f = \frac{k_1}{k_2 + k_1}$ and is the distribution of normalized reduction during anoxic conditions. The expected

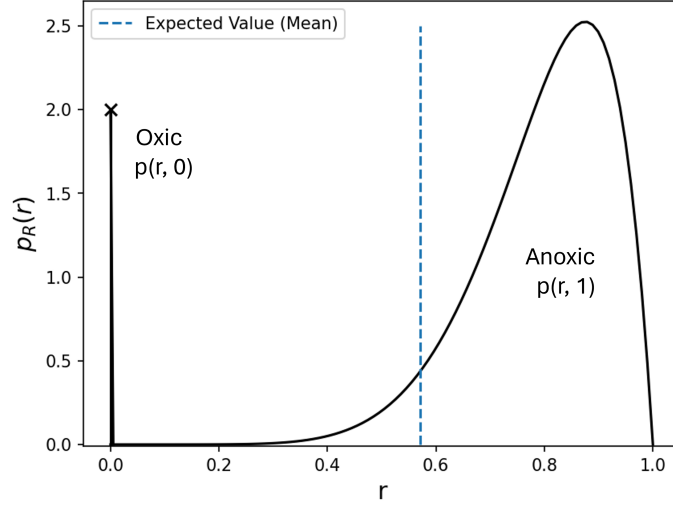


Figure 4.3: The PDF of normalized reduction rate, $p_R(r)$, is plotted from equation (4.47). At $r = 0$ is there is an atom of probability corresponding to oxic conditions. Parameters used are $k_o, k_r, k_1, k_2 = 1, 0.05, 1, 0.4$, all in [1/day].

value (mean) of this distribution can be calculated to obtain

$$\mathbf{E}[R] = \int_0^1 r' p_R(r') dr' = \frac{\beta \theta \phi}{(\theta + \phi + 1)(\theta + \phi + (\beta - 1)\phi)}. \quad (4.48)$$

Now that the PDF and expected value of the normalized variable, r , have been found, the average reduction and decomposition rates can be found by un-normalizing

$$\text{RED} = r \text{Fe}^{\text{tot}} k_r. \quad (4.49)$$

Now, assuming SOM is not limiting

$$\overline{\text{DEC}_{Fe}} = \overline{\text{RED}} \Omega = \mathbf{E}[R] \text{Fe}^{\text{tot}} k_r \Omega \quad (4.50)$$

where Ω is the mass of carbon oxidized per gram of Fe^{3+} reduced, and DEC_{Fe} is the mass of carbon oxidized by iron in g/kg/day.

4.5 Average Protection Capacity

Similarly to reduction, the PDF of x can be used to derive the expected value of soil protection capacity of carbon by reactive iron oxides. The protection capacity (PC) in the complete model given in equation (3.20) as

$$\text{PC} = \omega\text{Fe}^{3+} = \omega\text{Fe}^{\text{tot}}(1 - x). \quad (4.51)$$

Because PC is a linear function of x , the expectation of PC is simply

$$\mathbf{E}[\text{PC}] = \omega\text{Fe}^{\text{tot}}(1 - \mathbf{E}[x]), \quad (4.52)$$

where the expectation of x is known from equation (4.23). The maximum protection capacity is given by $\omega\text{Fe}^{\text{tot}}$. The PDF of % of maximum protection capacity is visible by simply flipping the PDFs in figure 4.1 around the $x = 0.5$ line.

4.6 Results and Discussion

4.6.1 Overview

In this section the dynamics of the iron cycle driven by DMN switching between redox states were solved at steady-state. This was done by first reducing the system to a single variable, x , representing the fraction of reactive iron that is present as Fe^{2+} . Then the problem was framed as an SDE (equation (4.6)) and solved in steady-state using the forward Kolmogorav equation [102]. The steady-state PDF of x is given by equation (4.16) and it was determined that three dimensionless parameters can describe the system: $\beta = k_o/k_r$, $\phi = k_1/k_o$, and $\theta = k_2/k_r$.

To determine k_1 and k_2 from soil and hydrological parameters a minimalist soil

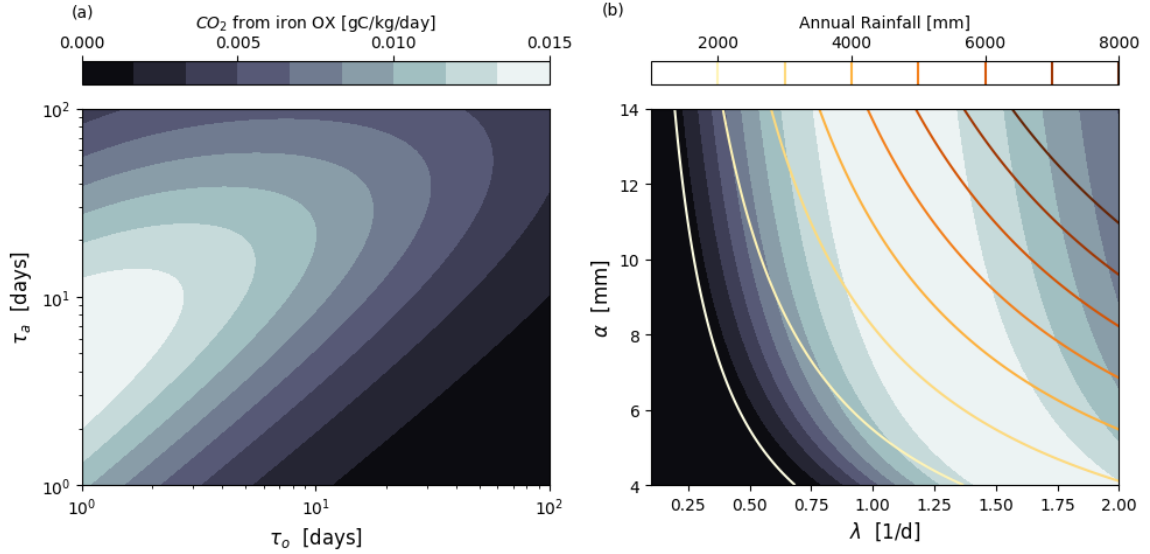


Figure 4.4: Contour plots of the expected value of carbon that can be oxidized by iron reduction for different hydrologic parameters. The constants used are $k_o = 1$, $k_r = 0.02 \text{ d}^{-1}$, $\text{Fe}^{\text{tot}} = 20 \text{ g/kg}$ and the soil parameters found in table 3.2. Z_r was adjusted from 0.4 to 0.8 m in plot (b). The x and y-axis on plot (a) are the mean duration of oxic periods, $\tau_o = 1/k_1$, and anoxic periods, $\tau_a = 1/k_2$ respectively. The x and y-axis on plot (b) are the frequency of rainfall λ in [1/day] and mean depth of rainfall α in mm. Level sets of total annual rainfall for values of α and λ are shown for (b).

moisture model was employed with stochastic rainfall [98]. Using crossing time statistics the mean duration of an oxic and anoxic period were determined, τ_o and τ_a respectively. Since $k_1 = 1/\tau_o$ and $k_2 = 1/\tau_a$ the PDF of x can be directly linked to hydrologic parameters such as rainfall depth, rain frequency, evapotranspiration, and soil depth. Figure 4.2 shows that the simplified soil moisture model (black line in (b)) and simplified stochastic model (black line in (d)) can estimate quite well while the complex system driven by the full soil moisture model.

The PDF of x was then used to investigate the potential of iron to be used as an oxidant in different climates. This was done by finding the PDF and expectation of the normalized reduction rate, r (equation (4.47)). In a similar manner the PDF of x was used to determine the distribution and expectation of protection capacity, PC, of carbon by iron oxides in the soil for a given pool of reactive iron and protection ratio, ω (equation (4.51)). The hydrological parameters determine r and x , but ultimately k_r ,

ω , and Fe^{tot} exert major control on both protection capacity and reduction capacity.

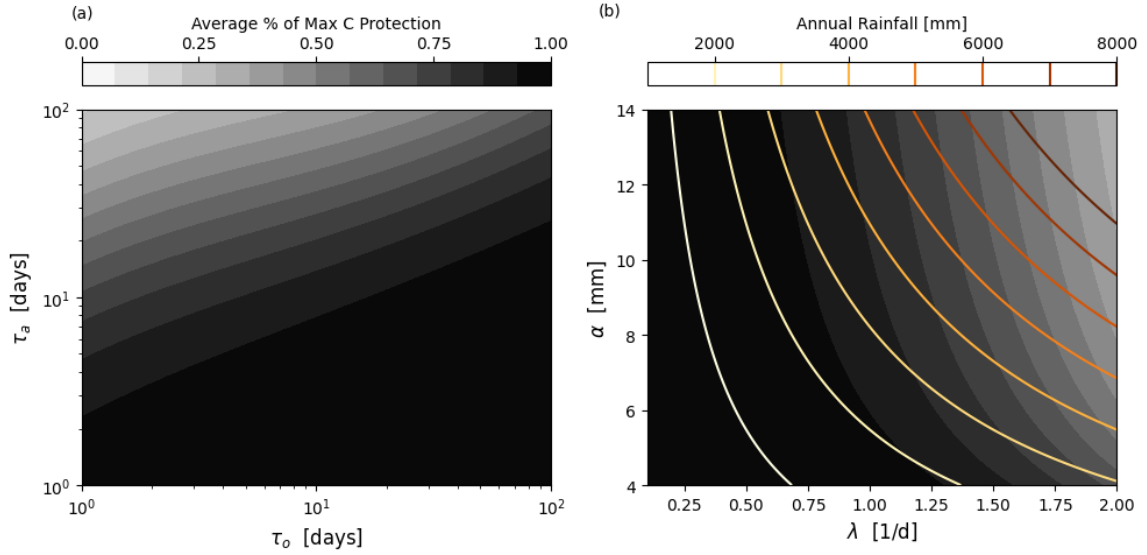


Figure 4.5: Contour plots of the average % of maximum protection capacity, equivalent to $\text{Fe}^{\text{tot}}\omega$ that is available from SROs. Mathematically it is $(\mathbf{E}[1 - x])$. %100 is entirely oxic conditions when all iron is reduced and 0% is entirely anoxic conditions when no reactive iron can protect carbon. (a) shows the effect of the average duration of anoxic and oxic periods. (b) shows the impact of rainfall mean and duration. The constants used are $k_o = 1$ and $k_r = 0.02 \text{ d}^{-1}$ and the soil parameters found in table 3.2. Z_r was adjusted from 0.4 to 0.8 m.

4.6.2 Implications

The PDF of iron (equation (4.16)) has two possible singularities. If $k_1/k_o = \phi < 1$ the PDF diverges at $x = 0$ and if $k_2/k_r = \theta < 1$ the PDF diverges at $x = 1$. In words, this means that if the redox conditions fluctuate faster than oxidation or reduction occur ($\phi > 1$ and $\theta > 1$) then iron will most often be in an intermediate state with some fraction reduced. If fluctuations are slower than the rate of oxidation or reduction, then entirely oxidized or entirely reduced states will dominate. This makes $\phi = 1$ and $\theta = 1$ thresholds where the qualitative behavior of the distribution changes. In non-wetlands, oxic conditions usually dominate and $k_1 < k_2$. Oxidation is also typically faster than reduction by up to several orders of magnitude, so $k_o > k_r$. This means that in upland soils $\phi < 1$ and $\theta > 1$ which yields divergence at $x = 0$ and zero at

$x = 1$. This corresponds to iron oxides dominating, not a surprising result [31, 127]. This effect is visible in the top-left plot in figure 4.1.

In the case where $\beta \approx 1$, the expectation of x reduces to

$$\mathbf{E}[x] \approx \frac{\phi}{\phi + \theta}. \quad (4.53)$$

In words, this equations states that the average fraction of reduced iron increases with the ratio of k_1 (speed of leaving oxic conditions) to k_o (rate of oxidation). It also decreases with the ratio of k_2 (speed of leaving anoxic conditions) to k_r (rate of reduction). Because reduction and oxidation can both vary by orders of magnitudes, it is likely that even under similar hydrologic conditions the mean fraction of reduction can be dramatically different.

The fraction of iron that is reduced is important for the ecological and pedogenic iron cycle. Plant uptake of iron can only occur when iron is aqueous. Fe^{2+} is orders of magnitudes more soluble than Fe^{3+} and thus the iron availability to plants depends directly on x [28]. There are other strategies to obtain iron such as releasing acid into the soil to dissolve it, but this requires the expenditure of resources by the plant [28]. Iron leaching in the soils also only occurs in the aqueous phase and as such a high average x leads to high leaching values as seen in [127] and [147].

The fraction of ferrous iron plays a significant role in the carbon dynamics in wet soils such as in rain forests or wetlands. Figure 4.4 shows the average daily CO_2 emissions value in gC/kg/day from iron reduction alone given a soil with 20 g/kg of reactive iron, non-limiting carbon inputs, and a reduction rate of $k_r = 0.02 \text{ d}^{-1}$. The significance of this is that iron is often the most energetically favourable oxidizer in anoxic soils and so its presence can stimulate carbon mineralization under certain conditions [12, 79]. Plot (a) in figure 4.4 shows the emissions from oxidation by iron as a function of the average length of oxic and anoxic periods. As visible there is a

peak for anoxic periods between 2 and 10 days with short oxic periods. As the anoxic periods get longer (τ_a increases) reduction decreases because iron becomes limiting. The shape of the plot suggests that for given k_o and k_r values there is an optimal trajectory that maximizes reduction. Calabrese et al. 2020 found that the limit of maximum reduction rate per cycle in the case of constant length cycles occurs as $\tau_a + \tau_o \rightarrow 0$ [21]. This agrees with this thesis' findings, but the reduction rate used here is averaged over all conditions including oxic and as such has a different maximum.

Plot (b) in figure 4.4 shows the same contours but as a function of rainfall frequency and mean rainfall depth. As visible, with higher rainfall frequency a maximum amount of reduction is achieved but beyond a certain level of rainfall the anoxic periods get too long and reduction decreases again. The bands in (b) show total annual rainfall. For reference, rainforests are considered to begin at 2000 mm of rain per year, with very few locations on Earth exceeding 6000 mm per year [55]. (b) is shown for specific values of soil rooting depth, evapotranspiration, porosity, field capacity, etc. and changing these properties can dramatically change the soil moisture and thus redox dynamics [99]. The goal of displaying charts (a) and (b) together is to connect soils in humid environments which undergo redox fluctuations due to rainfall and soils which are flooded seasonally or perennially by natural or manmade causes leading to longer redox cycles [147]. Both types of environments are critical stores of soil carbon and their redox dynamics are often considered separately, however the same fundamental processes are occurring in both [8, 16, 50, 59, 125, 134, 145].

Figure 4.5 shows the average fraction of maximum C protection capacity that is available as a function of (an)oxic excursion times (a) and rainfall parameters (b). This is a mirror of figure 4.4, in that it shows the role of iron as a protecting agent rather than a catalyst of decomposition. As visible the protection capacity of the soil increases with oxic conditions and decreases with anoxic conditions. The bottom left

corner in (a), quickly fluctuating redox conditions, shows a high protection capacity. In (b) only soils that are extremely wet, raining more than once a day on average ($\lambda > 1$), is there a decrease in protective capacity. It is visible however, that under extended anoxic conditions (high τ_a) it is expected that the protection capacity of the soil decreases. This agrees with LaCroix et al. 2019 which found that reactive iron content is correlated with carbon storage in upland soils (no extended anoxia) but not correlated in seasonally flooded lowland soils [70]. Considering figures 4.4 and 4.5 together, extended periods of anoxia on the order of about ten or more days would lead to iron reduction causing the release of MAOM and serving as an oxidant – both effects increasing CO₂ emissions. In a perennial wetland, however, iron would be fully reduced and thus thermodynamic limitations would take over and suppress decomposition (upper left corner (a) in figure 4.4).

Table 4.1: List of variables used in chapter 4.

Variable	Symbol	Unit
Fraction of reactive iron as Fe^{2+}	x	
First order rate constant oxidation	k_o	d^{-1}
First order rate constant reduction	k_r	d^{-1}
Frequency of switching from oxic to anoxic	k_1	d^{-1}
Frequency of switching from anoxic to oxic	k_2	d^{-1}
DMN driving variable representing redox state	ξ	
Dimensionless parameter k_o/k_r	β	
Dimensionless parameter k_1/k_o	ϕ	
Dimensionless parameter k_2/k_r	θ	
Effective relative soil moisture	y	
Maximum effective soil moisture	s_l	
Effective storage capacity of soil	w_o	m
Normalized evapotranspiration	η	
Reciprocal of normalized rainfall depth	γ	
Mean depth of rainfall	α	(m)m
Mean frequency of rainfall	λ	d^{-1}
Mean duration of oxic period	τ_o	d
Mean duration of anoxic period	τ_a	d
Fraction of time in anoxic	f	
Moisture threshold between anoxic and oxic	$s_c (y_c)$	
Normalized rate of reduction	r	
Carbon oxidation per iron reduction	Ω	gC/gFe
Carbon protection capacity of iron	PC	gC/kg
Carbon protection per unit of iron	ω	gC/gFe

Chapter 5

Conclusion

5.1 Key Points

- Iron addition to soil can increase or decrease carbon emissions depending on the ratio of the rates of reduction and oxidation to the speed of redox fluctuations.
- The interaction of the iron and carbon cycles depends heavily on the size of the reactive pool of iron in the soil (Fe^{tot}).
- The results of short-term experiments on carbon emissions from mineral soils should not be extrapolated to longer time frames.
- The novel PDF of the fraction of ferrous iron has many potential applications, e.g. modeling the leaching of iron from soils or helping predict carbon protection capacity.
- Under fast redox fluctuations, as in a humid upland soil, protection of carbon from iron oxides is likely maintained, but iron can still be an important oxidant.

5.2 Summary

The objective of this thesis was to untangle the hydrologic-iron-carbon cycles to improve the current understanding of this complex system. Several studies have investigated this issue by reviewing the mechanisms at play [36, 62, 118] and by running experiments [23, 58, 88, 93, 134]. Modeling the system is difficult, however, due to its complexity and sensitivity to local conditions. The simple model developed here hones in on two effects that are independently well studied, but whose dynamics have not yet been considered together in a model [22, 124]. The first effect is the role of iron as an electron acceptor/oxidant, which stimulates the decomposition of SOM in anoxic conditions [22, 28, 78, 125]. The second is the role of iron as a source of protection for SOM via sorption or co-precipitation [66]. These two processes intersect during the reduction of short-range iron oxides. These poorly crystalline minerals are associated with global carbon protection but are also the most readily reducible due to their high surface area [26, 66, 70, 101, 144]. Thus, the reactive pool of iron in the soils is a double-edged sword and its net impact depends on redox fluctuations and local conditions.

The numerical model developed in chapter 3 included pools for Fe^{3+} , Fe^{2+} , available carbon, and mineral-associated carbon. The iron and carbon cycles were coupled by the reduction term, which reduces Fe^{3+} while oxidizing carbon to CO_2 , and by the protection term, where the protection capacity of the soil was proportional to the Fe^{3+} pool. The simulations of the model demonstrate that different conditions can lead to contrasting effects on carbon decomposition. For instance, iron addition can lead to greater CO_2 emissions or less CO_2 emissions depending on the length of oxic versus anoxic conditions (figure 3.2). The kinetics of reduction were complicated by a feedback effect wherein iron reduction freed carbon that then increased the rate of iron reduction. The most important practical takeaway from these simulations is that

timescales are of utmost importance. Experiments that observe decreases in carbon emissions after ten or twenty days in anoxic conditions may simply not have had the time for the release of carbon caused by iron reduction to have an effect, as seen in [58]. The conundrum of time-scales is critical to global carbon storage efforts and understanding the mechanisms at play is a critical tool to predict long term greenhouse gas emission from soil [81, 139].

Much of the past work in studying the role of redox cycles on iron has considered redox cycles of constant length [21, 46, 88, 124]. In reality, redox cycles are driven by rainfall, which is a pseudo-random process, or streamflow, which can have high variability [109]. Thus, redox cycles are rarely truly of constant length. The goal of chapter 4 was to analyze the iron cycle in a steady state assuming it is forced by stochastic switches between redox conditions. Analytical solutions are desirable, as they pose clear relations that are easy to visualize and interpret. To solve the system analytically, it was simplified to a single SDE with a state variable $x = \text{Fe}^{2+}/\text{Fe}^{\text{tot}}$, where Fe^{tot} was assumed to be constant. The steady-state PDF of x and its mean were derived as a function of four physical parameters: k_o , k_r , k_1 , and k_2 which are the rate of oxidation, the rate of reduction, the rate of switching from oxic to anoxic conditions, and the rate of switching from anoxic to oxic conditions respectively. These four parameters were reduced to three key dimensionless parameters that govern the system: $\beta = k_o/k_r$, $\phi = k_1/k_o$, and $\theta = k_2/k_r$. A simplified soil moisture model was then used to derive k_1 and k_2 from soil and rainfall variables. Taken together, this allows one to find the PDF of x for *any* soil if its properties and the hydrologic conditions are known. This can inform iron availability to plants and the amount of iron leaching. Because reduction is a function of iron availability, the average reduction rate and thus the average carbon oxidation rate by iron can be found (figure 4.4). For the sample conditions used, it was found that average reduction would be maximized if anoxic conditions are between two to ten days and oxic periods are short (figure

4.4). If anoxic conditions are too long, iron limitations will reduce the average rate of reduction. The PDF of x can also inform the average protection capacity of iron in the soil, and it was found that protection remains near full under quickly fluctuating redox conditions (e.g. rain forest soils), even when anoxic conditions are more prevalent.

5.3 Limitations and Future Work

The primary limitation of this study is the simplified nature of the model used. Many effects, including iron toxicity, fenton reactions, pH, microbial dynamics, alternate electron acceptors, sorption effects on the rate of reduction, physical aggregation, anoxic microsites, rhizosphere dynamics, and dynamic crystallization, were not considered [2, 23, 51, 56, 57, 62, 66, 67, 118, 124, 140]. Some of these effects, such as microbial dynamics and pH, are included implicitly in the parameters of the model but considered approximately static—which may or may not fundamentally change the dynamics of the system. Future work should try to construct models that include more effects while preserving interpretability.

The other limitation of this thesis is that the results were not fit to data, and as such, the underlying structure of the model was not verified. Future work should address this by fitting both the numerical model and the solutions of the stochastic model to data. Possible starting points are data from experiments such as [88], [46], [3], and [23]. The solutions to the stochastic model are parsimonious and, in theory, can be applied to wetlands or soils around the world as long as their first order reduction and oxidation rates (k_r and k_o) and hydrologic properties are known. If in the future measurements of k_r and k_o for various soils become known, it will be possible to test the results of the stochastic model.

Major uncertainties remain about the future of SOM under climate change [11,

103, 123, 137]. A pressing question is the fate of the Gigatons of carbon stored in soils and how changing temperature and precipitation patterns will affect it [123]. To answer this question without decadal studies on the fate of carbon under different soil conditions, models that accurately capture the mechanisms of conservation are necessary. The emerging conception of mineral protection as an important factor in stabilizing carbon needs to be further modeled to understand the consequences of land use change and changes in precipitation [81, 139]. The iron cycle has varied interactions with soil carbon storage, raising the critical questions of why, when, and where the iron cycle will contribute to carbon storage in both positive and negative ways. This thesis attempted to elucidate the role of key time scales, parameters, initial conditions, and stochasticity in the coupled hydrologic-iron-carbon cycle through simple models. Future work should build on this modeling effort to improve our understanding and of the ferrous wheel and its effect on the carbon cycle.

Chapter 6

Appendix

6.1 Appendix A: Assumption of a Constant Reactive Iron Pool.

The approximation of constant reactive iron is reasonable given that the rate of leaching from soils ($\frac{d\text{Fe}^{\text{tot}}}{dt}$) is significantly lower in most conditions than the rate of reduction and oxidation. Data from Thompson et al. 2011 on iron along a rainfall gradient in Hawaii suggests a leaching rate on the order of $1 \times 10^{-5} \text{ g kg}^{-1} \text{ d}^{-1}$ at 4200 mm of rain per year [127]. At the high end of global rainfall, this ecosystem gives an approximate upper bound on leaching in upland soils exposed to heavy rain. Another paper by Chen et al. 2022 estimating iron leaching from paddy soils in China, where flooding creates ideal leaching conditions, found a maximum rate of leaching within the first decades of irrigating an upland soil to be on the order of 10^{-3} g/kg/day [27]. The sudden flooding of upland soils should give a good upper bound on maximum possible leaching in any natural soil. The leaching of Fe^{2+} is thought to encourage the dissolution of more stable and crystalline iron oxides, increasing the pool of readily reducible iron oxides [106, 127]. Thus even when leaching is non-negligible, this process helps maintain a quasi steady pool of reactive iron [106, 127].

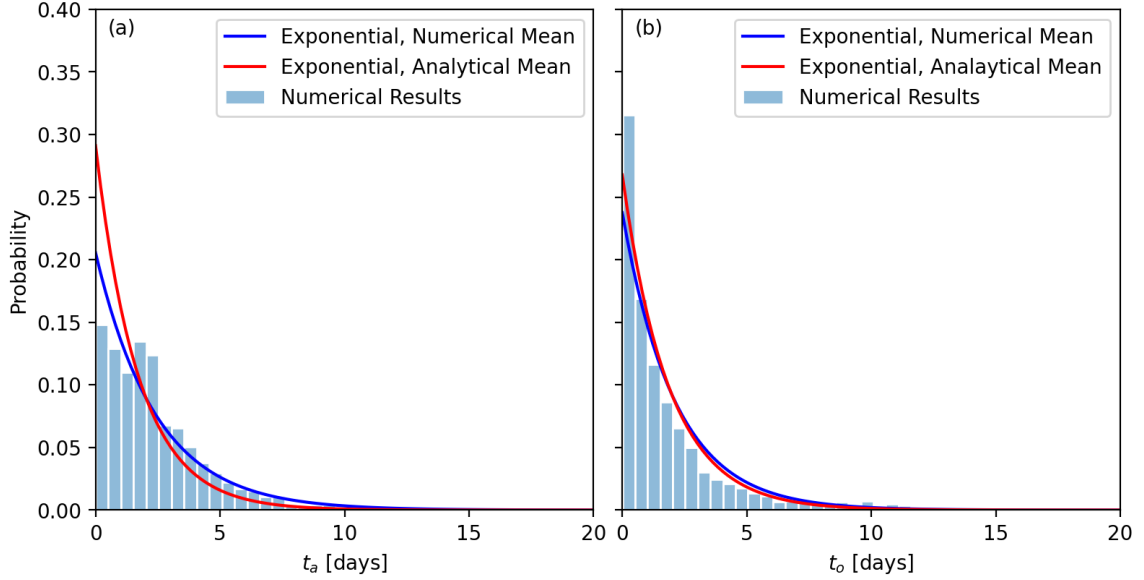


Figure 6.1: (a) The distribution of the duration of anoxic period, t_a , with mean τ_a . (b) The distribution of the duration of anoxic period, t_o , with mean τ_o . The histograms come from the crossing times of a 10,000 day simulation with parameters $\alpha = 12$ mm and $\lambda = 0.82$ d⁻¹.

6.2 Appendix B: Assumption of Exponential Crossing Times

In making the assumption that the system is driven by DMN, it was implicitly assumed that crossing times are Markovian, i.e. the time until crossing does not depend on the previous time until crossing and is equally likely at any point in time. This assumption would lead crossing times to be exponentially distributed. In actuality and in the model of soil moisture used the crossing times are not completely random but are in fact driven by both the stochastic rain inputs and deterministic soil moisture dynamics. k_1 and k_2 were derived from soil moisture dynamics by taking the reciprocal of the mean excursion time below and above the oxic threshold, $\mathbf{E}[t_o] = \tau_o$ and $\mathbf{E}[t_a] = \tau_a$ respectively. This gives the correct average value, however knowing the expected values does not imply that the excursion times t_o and t_a are exponentially distributed, this must be verified separately. Figure 6.1 shows the distribution

of duration of excursions in anoxic (a) and oxic (b) over 10,000 days. The numerical simulation was run using the complete soil moisture model (section 3.1). The mean value of soil moisture is taken from the simulation and plotted as an exponential curve (blue line). The simplified soil moisture model was also used to predict crossing times using equation (4.36) and an exponential distribution was plotted (red line). As visible in (a) both exponential fits overestimate the proportion of short excursions into anoxic conditions and underestimate the amount of excursions around 3 days long. In (a) the numerical mean has a better fit as it has a larger mean than the simplified analytical prediction. In (b) the exponential curves have a good fit and both the predicted mean and the numerical mean provide good approximations. These results suggest that an exponential distribution of crossing times and thus DMN is an *okay* assumption for the switches between oxic and anoxic conditions.

Bibliography

1. Abramowitz, M. *Handbook of mathematical functions : with formulas, graphs, and mathematical tables* English (ed Stegun, I. A.) ISBN: 978-0-486-61272-0 (New York: Dover Publications, 1965).
2. Achtnich, C., Bak, F. & Conrad, R. Competition for electron donors among nitrate reducers, ferric iron reducers, sulfate reducers, and methanogens in anoxic paddy soil. en. *Biology and Fertility of Soils* **19**, 65–72. ISSN: 1432-0789 (Jan. 1995).
3. Adhikari, D. *et al.* Dynamics of ferrihydrite-bound organic carbon during microbial Fe reduction. *Geochimica et Cosmochimica Acta* **212**, 221–233. ISSN: 0016-7037 (Sept. 2017).
4. Agren, G. I. & Bosatta, E. *Theoretical Ecosystem Ecology: Understanding Element Cycles* en. ISBN: 978-0-521-64651-2 (Cambridge University Press, July 1998).
5. Amstaetter, K., Borch, T. & Kappler, A. Influence of humic acid imposed changes of ferrihydrite aggregation on microbial Fe(III) reduction. *Geochimica et Cosmochimica Acta* **85**, 326–341. ISSN: 0016-7037 (May 2012).
6. Bailey, V. L., Pries, C. H. & Lajtha, K. What do we know about soil carbon destabilization? en. *Environmental Research Letters* **14**. 083004. ISSN: 1748-9326 (July 2019).
7. Barcellos, D., Cyle, K. T. & Thompson, A. Faster redox fluctuations can lead to higher iron reduction rates in humid forest soils. en. *Biogeochemistry* **137**, 367–378. ISSN: 1573-515X (Feb. 2018).
8. Barcellos, D., O’Connell, C. S., Silver, W., Meile, C. & Thompson, A. Hot Spots and Hot Moments of Soil Moisture Explain Fluctuations in Iron and Carbon Cycling in a Humid Tropical Forest Soil. en. *Soil Systems* **2**. 59. ISSN: 2571-8789 (Dec. 2018).
9. Barros, N. Thermodynamics of Soil Microbial Metabolism: Applications and Functions. en. *Applied Sciences* **11**. 4962. ISSN: 2076-3417 (Jan. 2021).
10. Benner, S. G., Hansel, C. M., Wielinga, B. W., Barber, T. M. & Fendorf, S. Reductive Dissolution and Biomineralization of Iron Hydroxide under Dynamic Flow Conditions. *Environmental Science & Technology* **36**. 1705–1711. ISSN: 0013-936X (Apr. 2002).
11. Berardi, D. *et al.* 21st-century biogeochemical modeling: Challenges for Century-based models and where do we go from here? en. *GCB Bioenergy* **12**. 774–788. ISSN: 1757-1707 (2020).

12. Bethke, C. M., Sanford, R. A., Kirk, M. F., Jin, Q. & Flynn, T. M. The thermodynamic ladder in geomicrobiology. *American Journal of Science* **311**, 183–210. ISSN: 0002-9599 (Mar. 2011).
13. Beven, K. A manifesto for the equifinality thesis. *Journal of Hydrology. The model parameter estimation experiment* **320**, 18–36. ISSN: 0022-1694 (Mar. 2006).
14. Beven, K. en. in *Computer Simulation Validation: Fundamental Concepts, Methodological Frameworks, and Philosophical Perspectives* (eds Beisbart, C. & Saam, N. J.) 791–809 (Springer International Publishing, Cham, 2019). ISBN: 978-3-319-70766-2.
15. Beven, K. & Freer, J. Equifinality, data assimilation, and uncertainty estimation in mechanistic modelling of complex environmental systems using the GLUE methodology. *Journal of Hydrology* **249**, 11–29. ISSN: 0022-1694 (Aug. 2001).
16. Bhattacharyya, A. *et al.* Redox Fluctuations Control the Coupled Cycling of Iron and Carbon in Tropical Forest Soils. *Environmental Science & Technology* **52**. 14129–14139. ISSN: 0013-936X (Dec. 2018).
17. Bloomfield, J., Vogt, K. A. & Vogt, D. J. Decay rate and substrate quality of fine roots and foliage of two tropical tree species in the Luquillo Experimental Forest, Puerto Rico. en. *Plant and Soil* **150**, 233–245. ISSN: 1573-5036 (Mar. 1993).
18. Bonneville, S., Behrends, T., Cappellen, P. V., Hyacinthe, C. & Röling, W. F. M. Reduction of Fe(III) colloids by *Shewanella putrefaciens*: A kinetic model. *Geochimica et Cosmochimica Acta. A Special Issue Dedicated to Robert A. Berner* **70**, 5842–5854. ISSN: 0016-7037 (Dec. 2006).
19. Bonneville, S., Van Cappellen, P. & Behrends, T. Microbial reduction of iron(III) oxyhydroxides: effects of mineral solubility and availability. *Chemical Geology. Bacteria and Geochemical Speciation of Metals* **212**, 255–268. ISSN: 0009-2541 (Dec. 2004).
20. Buckingham, E. On Physically Similar Systems; Illustrations of the Use of Dimensional Equations. *Physical Review* **4**. 345–376 (Oct. 1914).
21. Calabrese, S., Barcellos, D., Thompson, A. & Porporato, A. Theoretical Constraints on Fe Reduction Rates in Upland Soils as a Function of Hydroclimatic Conditions. en. *Journal of Geophysical Research: Biogeosciences* **125**, e2020JG005894. ISSN: 2169-8953, 2169-8961 (Dec. 2020).
22. Calabrese, S. & Porporato, A. Impact of ecohydrological fluctuations on iron-redox cycling. en. *Soil Biology and Biochemistry* **133**, 188–195. ISSN: 00380717 (June 2019).
23. Chen, C., Hall, S. J., Coward, E. & Thompson, A. Iron-mediated organic matter decomposition in humid soils can counteract protection. en. *Nature Communications* **11**. 2255. ISSN: 2041-1723 (May 2020).
24. Chen, H. *et al.* Effects of nitrogen deposition on soil sulfur cycling. en. *Global Biogeochemical Cycles* **30**. 1568–1577. ISSN: 1944-9224 (Nov. 2016).

25. Chen, J.-L., Reynolds, J. F., Harley, P. C. & Tenhunen, J. D. Coordination theory of leaf nitrogen distribution in a canopy. *Oecologia* **93**, 63–69. ISSN: 0029-8549, 1432-1939 (Feb. 1993).
26. Chen, K.-Y. *et al.* Stabilization of Natural Organic Matter by Short-Range-Order Iron Hydroxides. *Environmental Science & Technology* **50**. 12612–12620. ISSN: 0013-936X (Dec. 2016).
27. Chen, L. *et al.* Iron loss of paddy soil in China and its environmental implications. en. *Science China Earth Sciences* **65**, 1277–1291. ISSN: 1869-1897 (July 2022).
28. Colombo, C., Palumbo, G., He, J.-Z., Pinton, R. & Cesco, S. Review on iron availability in soil: interaction of Fe minerals, plants, and microbes. en. *Journal of Soils and Sediments* **14**, 538–548. ISSN: 1614-7480 (Mar. 2014).
29. Conrad, R. Methane Production in Soil Environments—Anaerobic Biogeochemistry and Microbial Life between Flooding and Desiccation. en. *Microorganisms* **8**. 881. ISSN: 2076-2607 (June 2020).
30. Cooper, I., Mondal, A. & Antonopoulos, C. G. A SIR model assumption for the spread of COVID-19 in different communities. *Chaos, Solitons & Fractals* **139**, 110057. ISSN: 0960-0779 (Oct. 2020).
31. Cornell, R. M. & Schwertmann, U. *The Iron Oxides* ISBN: 978-3-527-30274-1 (Wiley Only Books, 2003).
32. Cotrufo, M. F. & Lavalley, J. M. in *Advances in Agronomy* (ed Sparks, D. L.) 1–66 (Academic Press, Jan. 2022).
33. Cotrufo, M. F. *et al.* Formation of soil organic matter via biochemical and physical pathways of litter mass loss. en. *Nature Geoscience* **8**. 776–779. ISSN: 1752-0908 (Oct. 2015).
34. Cutting, R. S., Coker, V. S., Fellowes, J. W., Lloyd, J. R. & Vaughan, D. J. Mineralogical and morphological constraints on the reduction of Fe(III) minerals by *Geobacter sulfurreducens*. *Geochimica et Cosmochimica Acta* **73**, 4004–4022. ISSN: 0016-7037 (July 2009).
35. D’Odorico, P., Laio, F. & Ridolfi, L. Noise-induced stability in dryland plant ecosystems. en. *Proceedings of the National Academy of Sciences* **102**, 10819–10822. ISSN: 0027-8424, 1091-6490 (Aug. 2005).
36. Dong, H. *et al.* Coupled iron cycling and organic matter transformation across redox interfaces. en. *Nature Reviews Earth & Environment* **4**. 659–673. ISSN: 2662-138X (Sept. 2023).
37. Dubinsky, E. A., Silver, W. L. & Firestone, M. K. Tropical forest soil microbial communities couple iron and carbon biogeochemistry. en. *Ecology* **91**. 2604–2612. ISSN: 1939-9170 (2010).
38. Duckworth, O. W., Holmström, S. J. M., Peña, J. & Sposito, G. Biogeochemistry of iron oxidation in a circumneutral freshwater habitat. *Chemical Geology* **260**, 149–158. ISSN: 0009-2541 (Mar. 2009).
39. Dynarski, K. A., Bossio, D. A. & Scow, K. M. Dynamic Stability of Soil Carbon: Reassessing the “Permanence” of Soil Carbon Sequestration. *Frontiers in Environmental Science* **8**. ISSN: 2296-665X (2020).

40. Ekman, V. W. A Survey of some Theoretical Investigations on Ocean-Currents. *ICES Journal of Marine Science* **3**, 295–327. ISSN: 1054-3139 (Dec. 1928).
41. Emsens, W.-J. *et al.* Soil Iron Content as a Predictor of Carbon and Nutrient Mobilization in Rewetted Fens. en. *PLOS ONE* **11**. e0153166. ISSN: 1932-6203 (Apr. 2016).
42. Eriksson, E. Compartment Models and Reservoir Theory. *Annual Review of Ecology and Systematics* **2**. 67–84. ISSN: 0066-4162 (1971).
43. Fontaine, S., Mariotti, A. & Abbadie, L. The priming effect of organic matter: a question of microbial competition? *Soil Biology and Biochemistry* **35**, 837–843. ISSN: 0038-0717 (June 2003).
44. Freeze, A. R. & Cherry, J. A. *Groundwater* (Prentice-Hall, Englewood Cliffs, N.J., 1979).
45. Georgiou, K. *et al.* Global stocks and capacity of mineral-associated soil organic carbon. en. *Nature Communications* **13**. 3797. ISSN: 2041-1723 (July 2022).
46. Ginn, B., Meile, C., Wilmoth, J., Tang, Y. & Thompson, A. Rapid Iron Reduction Rates Are Stimulated by High-Amplitude Redox Fluctuations in a Tropical Forest Soil. *Environmental Science & Technology* **51**. 3250–3259. ISSN: 0013-936X (Mar. 2017).
47. Glusker, J. P. Mechanism of aconitase action deduced from crystallographic studies of its substrates. *Journal of Molecular Biology* **38**, 149–162. ISSN: 0022-2836 (Dec. 1968).
48. Greenwood, D. J. The Effect of Oxygen Concentration on the Decomposition of Organic Materials in Soil. *Plant and Soil* **14**. 360–376. ISSN: 0032-079X (1961).
49. Gunina, A. & Kuzyakov, Y. From energy to (soil organic) matter. en. *Global Change Biology* **28**. 2169–2182. ISSN: 1365-2486 (2022).
50. Hall, S. J., McDowell, W. H. & Silver, W. L. When Wet Gets Wetter: Decoupling of Moisture, Redox Biogeochemistry, and Greenhouse Gas Fluxes in a Humid Tropical Forest Soil. en. *Ecosystems* **16**, 576–589. ISSN: 1435-0629 (June 2013).
51. Hall, S. J. & Silver, W. L. Iron oxidation stimulates organic matter decomposition in humid tropical forest soils. en. *Global Change Biology* **19**. 2804–2813. ISSN: 1365-2486 (2013).
52. Hansel, C. M., Benner, S. G., Nico, P. & Fendorf, S. Structural constraints of ferric (hydr)oxides on dissimilatory iron reduction and the fate of Fe(II)₃. *Geochimica et Cosmochimica Acta. A Special Issue on Microbial Geochemistry* **68**, 3217–3229. ISSN: 0016-7037 (Aug. 2004).
53. Hemingway, J. D. *et al.* Mineral protection regulates long-term global preservation of natural organic carbon. en. *Nature* **570**. 228–231. ISSN: 1476-4687 (June 2019).
54. Henneron, L. *et al.* Bioenergetic control of soil carbon dynamics across depth. en. *Nature Communications* **13**. 7676. ISSN: 2041-1723 (Dec. 2022).
55. Holdridge, L. R. Life Zone Ecology. *Life Zone Ecology* (1967).
56. Hua, J., Sun, J., Chen, M., Liu, C. & Wu, F. Aqueous Fe(II)-catalyzed iron oxide recrystallization: Fe redox cycling and atom exchange, mineralogical re-

- crystallization and contributing factor. en. *Reviews in Environmental Science and Bio/Technology* **22**, 55–78. ISSN: 1572-9826 (Mar. 2023).
57. Huang, J. *et al.* Fe(II) Redox Chemistry in the Environment. *Chemical Reviews* **121**. 8161–8233. ISSN: 0009-2665 (July 2021).
 58. Huang, W. & Hall, S. J. Elevated moisture stimulates carbon loss from mineral soils by releasing protected organic matter. en. *Nature Communications* **8**. 1774. ISSN: 2041-1723 (Nov. 2017).
 59. Jia, B., Niu, Z., Wu, Y., Kuzyakov, Y. & Li, X. G. Waterlogging increases organic carbon decomposition in grassland soils. *Soil Biology and Biochemistry* **148**, 107927. ISSN: 0038-0717 (Sept. 2020).
 60. Jin, Q. & Kirk, M. F. pH as a Primary Control in Environmental Microbiology: 1. Thermodynamic Perspective. English. *Frontiers in Environmental Science* **6**. ISSN: 2296-665X (May 2018).
 61. Johnson, N. L. *Continuous univariate distributions* 2nd ed. English (eds Kotz, S. & Balakrishnan, N.) ISBN: 978-0-471-58495-7 (New York: Wiley, 1994).
 62. Kappler, A. *et al.* An evolving view on biogeochemical cycling of iron. en. *Nature Reviews Microbiology* **19**. 360–374. ISSN: 1740-1534 (June 2021).
 63. Kendall, B., Anbar, A. D., Kappler, A. & Konhauser, K. O. en. in *Fundamentals of Geobiology* (eds Knoll, A. H., Canfield, D. E. & Konhauser, K. O.) 1st ed., 65–92 (Wiley, Apr. 2012). ISBN: 978-1-118-28081-2 978-1-118-28087-4.
 64. Kirsten, M. *et al.* Iron oxides and aluminous clays selectively control soil carbon storage and stability in the humid tropics. en. *Scientific Reports* **11**. 5076. ISSN: 2045-2322 (Mar. 2021).
 65. Kleber, M. What is recalcitrant soil organic matter? en. *Environmental Chemistry* **7**. 320–332. ISSN: 1449-8979 (Aug. 2010).
 66. Kleber, M. *et al.* in *Advances in Agronomy* (ed Sparks, D. L.) 1–140 (Academic Press, Jan. 2015).
 67. Kleber, M. *et al.* Dynamic interactions at the mineral–organic matter interface. en. *Nature Reviews Earth & Environment* **2**. 402–421. ISSN: 2662-138X (June 2021).
 68. Kusunoki, S., Ose, T. & Hosaka, M. Emergence of unprecedented climate change in projected future precipitation. en. *Scientific Reports* **10**. 4802. ISSN: 2045-2322 (Mar. 2020).
 69. Lacroix, E. M. *et al.* Mineral Protection and Resource Limitations Combine to Explain Profile-Scale Soil Carbon Persistence. en. *Journal of Geophysical Research: Biogeosciences* **127**. e2021JG006674. ISSN: 2169-8961 (2022).
 70. LaCroix, R. E. *et al.* Shifting mineral and redox controls on carbon cycling in seasonally flooded mineral soils. English. *Biogeosciences* **16**. 2573–2589. ISSN: 1726-4170 (July 2019).
 71. Laio, F., Porporato, A., Ridolfi, L. & Rodriguez-Iturbe, I. Plants in water-controlled ecosystems: active role in hydrologic processes and response to water stress: II. Probabilistic soil moisture dynamics. *Advances in Water Resources* **24**, 707–723. ISSN: 0309-1708 (July 2001).

72. LaRowe, D. E. & Van Cappellen, P. Degradation of natural organic matter: A thermodynamic analysis. *Geochimica et Cosmochimica Acta* **75**, 2030–2042. ISSN: 0016-7037 (Apr. 2011).
73. Le Quéré, C. *et al.* Global Carbon Budget 2018. English. *Earth System Science Data* **10**, 2141–2194. ISSN: 1866-3508 (Dec. 2018).
74. Lehmann, J. *et al.* Persistence of soil organic carbon caused by functional complexity. en. *Nature Geoscience* **13**, 529–534. ISSN: 1752-0908 (Aug. 2020).
75. Lens, F. *et al.* Functional xylem characteristics associated with drought-induced embolism in angiosperms. *New Phytologist* **236**, 2019–2036. ISSN: 0028-646X, 1469-8137 (Dec. 2022).
76. Lin, Y. *et al.* Differential effects of redox conditions on the decomposition of litter and soil organic matter. en. *Biogeochemistry* **154**, 1–15. ISSN: 1573-515X (May 2021).
77. Liu, L., Zheng, N., Yu, Y., Zheng, Z. & Yao, H. Soil carbon and nitrogen cycles driven by iron redox: A review. *Science of The Total Environment* **918**, 170660. ISSN: 0048-9697 (Mar. 2024).
78. Lovley, D. R. Organic matter mineralization with the reduction of ferric iron: A review. *Geomicrobiology Journal* **5**, 375–399. ISSN: 0149-0451 (Jan. 1987).
79. Lovley, D. R. Microbial Fe(III) reduction in subsurface environments. *FEMS Microbiology Reviews* **20**, 305–313. ISSN: 0168-6445 (July 1997).
80. Lovley, D. R., Phillips, E. J. P. & Lonergan, D. J. Enzymic versus nonenzymic mechanisms for iron(III) reduction in aquatic sediments. *Environmental Science & Technology* **25**, 1062–1067. ISSN: 0013-936X (June 1991).
81. Luo, Z., Baldock, J. & Wang, E. Modelling the dynamic physical protection of soil organic carbon: Insights into carbon predictions and explanation of the priming effect. en. *Global Change Biology* **23**, 5273–5283. ISSN: 1365-2486 (2017).
82. Lützw, M. v. *et al.* Stabilization of organic matter in temperate soils: mechanisms and their relevance under different soil conditions – a review. en. *European Journal of Soil Science* **57**, 426–445. ISSN: 1365-2389 (2006).
83. Manzoni, S., Katul, G. & Porporato, A. A dynamical system perspective on plant hydraulic failure. *Water Resources Research* **50**, 5170–5183 (2014).
84. Manzoni, S. & Porporato, A. Soil carbon and nitrogen mineralization: Theory and models across scales. en. *Soil Biology and Biochemistry* **41**, 1355–1379. ISSN: 00380717 (July 2009).
85. Marquart, K. A. *et al.* Influence of pH on the balance between methanogenesis and iron reduction. en. *Geobiology* **17**, 185–198. ISSN: 1472-4669 (2019).
86. Megonigal, J. P. & Guenther, A. B. Methane emissions from upland forest soils and vegetation. *Tree Physiology* **28**, 491–498. ISSN: 0829-318X (Apr. 2008).
87. Mentges, A., Feenders, C., Deutsch, C., Blasius, B. & Dittmar, T. Long-term stability of marine dissolved organic carbon emerges from a neutral network of compounds and microbes. en. *Scientific Reports* **9**, 17780. ISSN: 2045-2322 (Nov. 2019).

88. Mikutta, C. *et al.* Redox cycling of straw-amended soil simultaneously increases iron oxide crystallinity and the content of highly disordered organo-iron(III) solids. *Geochimica et Cosmochimica Acta*. ISSN: 0016-7037 (Feb. 2024).
89. Mikutta, R., Lorenz, D., Guggenberger, G., Haumaier, L. & Freund, A. Properties and reactivity of Fe-organic matter associations formed by coprecipitation *versus* adsorption: Clues from arsenate batch adsorption. *Geochimica et Cosmochimica Acta* **144**, 258–276. ISSN: 0016-7037 (Nov. 2014).
90. Notini, L. *et al.* A Closer Look at Fe(II) Passivation of Goethite. *ACS Earth and Space Chemistry* **3**. 2717–2725 (Dec. 2019).
91. Olson, J. S. Energy Storage and the Balance of Producers and Decomposers in Ecological Systems. *Ecology* **44**. 322–331. ISSN: 0012-9658 (1963).
92. Ostwald, W. Ostwald ripening. *Physical Chemistry* **34**, 495–503 (1900).
93. Pan, W., Kan, J., Inamdar, S., Chen, C. & Sparks, D. Dissimilatory microbial iron reduction release DOC (dissolved organic carbon) from carbon-ferrihydrite association. *Soil Biology and Biochemistry* **103**, 232–240. ISSN: 0038-0717 (Dec. 2016).
94. Parnas, H. A theoretical explanation of the priming effect based on microbial growth with two limiting substrates. *Soil Biology and Biochemistry* **8**, 139–144. ISSN: 0038-0717 (Jan. 1976).
95. Patzner, M. S. *et al.* Iron mineral dissolution releases iron and associated organic carbon during permafrost thaw. en. *Nature Communications* **11**. 6329. ISSN: 2041-1723 (Dec. 2020).
96. Plazinski, W., Rudzinski, W. & Plazinska, A. Theoretical models of sorption kinetics including a surface reaction mechanism: A review. *Advances in Colloid and Interface Science* **152**, 2–13. ISSN: 0001-8686 (Nov. 2009).
97. Porporato, A., D’Odorico, P., Laio, F. & Rodriguez-Iturbe, I. Hydrologic controls on soil carbon and nitrogen cycles. I. Modeling scheme. en. *Advances in Water Resources* **26**, 45–58. ISSN: 03091708 (Jan. 2003).
98. Porporato, A., Daly, E. & Rodriguez-Iturbe, I. Soil Water Balance and Ecosystem Response to Climate Change. *The American Naturalist* **164**. 625–632. ISSN: 0003-0147 (Nov. 2004).
99. Porporato, A. & Yin, J. *Ecohydrology* ISBN: 978-1-108-84054-5 (Cambridge University Press, 2022).
100. Powers, J. S. *et al.* Decomposition in tropical forests: a pan-tropical study of the effects of litter type, litter placement and mesofaunal exclusion across a precipitation gradient. en. *Journal of Ecology* **97**. 801–811. ISSN: 1365-2745 (2009).
101. Rasmussen, C. *et al.* Beyond clay: towards an improved set of variables for predicting soil organic matter content. en. *Biogeochemistry* **137**, 297–306. ISSN: 1573-515X (Feb. 2018).
102. Ridolfi, L., D’Odorico, P. & Laio, F. *Noise-Induced Phenomena in the Environmental Sciences* ISBN: 978-0-521-19818-9 (Cambridge University Press, 2011).
103. Riley, W. J. *et al.* en. in *Multi-Scale Biogeochemical Processes in Soil Ecosystems* 233–257 (John Wiley & Sons, Ltd, 2022). ISBN: 978-1-119-48041-9.

104. Roden, E. E. Fe(III) Oxide Reactivity Toward Biological versus Chemical Reduction. *Environmental Science & Technology* **37**. 1319–1324. ISSN: 0013-936X (Apr. 2003).
105. Roden, E. E. Analysis of long-term bacterial vs. chemical Fe(III) oxide reduction kinetics1. *Geochimica et Cosmochimica Acta. A Special Issue on Microbial Geochemistry* **68**, 3205–3216. ISSN: 0016-7037 (Aug. 2004).
106. Roden, E. E. Geochemical and microbiological controls on dissimilatory iron reduction. *Comptes Rendus Geoscience. Les hydroxydes ferrosiques, les rouilles vertes et la fougérite dans le cycle biogéochimique du fer* **338**, 456–467. ISSN: 1631-0713 (June 2006).
107. Roden, E. E. & Urrutia, M. M. Ferrous Iron Removal Promotes Microbial Reduction of Crystalline Iron(III) Oxides. *Environmental Science & Technology* **33**. 1847–1853. ISSN: 0013-936X (June 1999).
108. Roden, E. E., Urrutia, M. M. & Mann, C. J. Bacterial Reductive Dissolution of Crystalline Fe(III) Oxide in Continuous-Flow Column Reactors. *Applied and Environmental Microbiology* **66**. 1062–1065 (Mar. 2000).
109. Rodriguez-Iturbe, I., Porporato, A., Ridolfi, L., Isham, V. & Coxi, D. R. Probabilistic modelling of water balance at a point: the role of climate, soil and vegetation. *Proceedings of the Royal Society of London. Series A: Mathematical, Physical and Engineering Sciences* **455**. 3789–3805 (Oct. 1999).
110. Saaltink, M., Batlle, F., Ayora, C., Carrera, J. & Olivella, S. RETRASO, a code for modeling reactive transport in saturated and unsaturated porous media. English. *Geologica Acta* **2**, 235–251. ISSN: 1695-6133 (2004).
111. Schink, B. Microbially Driven Redox Reactions in Anoxic Environments: Pathways, Energetics, and Biochemical Consequences. en. *Engineering in Life Sciences* **6**. 228–233. ISSN: 1618-2863 (2006).
112. Shi, Z. *et al.* The age distribution of global soil carbon inferred from radiocarbon measurements. en. *Nature Geoscience* **13**. 555–559. ISSN: 1752-0908 (Aug. 2020).
113. Sierra, C. A. & Müller, M. A general mathematical framework for representing soil organic matter dynamics. en. *Ecological Monographs* **85**. 505–524. ISSN: 1557-7015 (2015).
114. Sierra, C. A., Müller, M., Metzler, H., Manzoni, S. & Trumbore, S. E. The muddle of ages, turnover, transit, and residence times in the carbon cycle. en. *Global Change Biology* **23**. 1763–1773. ISSN: 1365-2486 (2017).
115. Silver, W., Lugo, A. & Keller, M. Soil oxygen availability and biogeochemistry along rainfall and topographic gradients in upland wet tropical forest soils. en. *Biogeochemistry* **44**, 301–328. ISSN: 1573-515X (Mar. 1999).
116. Singer, P. C. & Stumm, W. Acidic Mine Drainage: The Rate-Determining Step. *Science* **167**. 1121–1123. ISSN: 0036-8075 (1970).
117. Slessarev, E. W. *et al.* Water balance creates a threshold in soil pH at the global scale. en. *Nature* **540**. 567–569. ISSN: 1476-4687 (Dec. 2016).
118. Song, X. *et al.* Towards a better understanding of the role of Fe cycling in soil for carbon stabilization and degradation. en. *Carbon Research* **1**, 5. ISSN: 2731-6696 (June 2022).

119. Soong, J. L. *et al.* Microbial carbon limitation: The need for integrating microorganisms into our understanding of ecosystem carbon cycling. en. *Global Change Biology* **26**. 1953–1961. ISSN: 1365-2486 (2020).
120. Sowerby, A., Emmett, B. A., Tietema, A. & Beier, C. Contrasting effects of repeated summer drought on soil carbon efflux in hydric and mesic heathland soils. en. *Global Change Biology* **14**. 2388–2404. ISSN: 1365-2486 (2008).
121. Stumm, W. & Sulzberger, B. The cycling of iron in natural environments: Considerations based on laboratory studies of heterogeneous redox processes. *Geochimica et Cosmochimica Acta* **56**, 3233–3257. ISSN: 0016-7037 (Aug. 1992).
122. Suarez, D. L. & Šimůnek, J. UNSATCHEM: Unsaturated Water and Solute Transport Model with Equilibrium and Kinetic Chemistry. en. *Soil Science Society of America Journal* **61**. 1633–1646. ISSN: 1435-0661 (1997).
123. Sulman, B. N. *et al.* Multiple models and experiments underscore large uncertainty in soil carbon dynamics. en. *Biogeochemistry* **141**, 109–123. ISSN: 1573-515X (Nov. 2018).
124. Sulman, B. N. *et al.* Simulated Hydrological Dynamics and Coupled Iron Redox Cycling Impact Methane Production in an Arctic Soil. en. *Journal of Geophysical Research: Biogeosciences* **127**. e2021JG006662. ISSN: 2169-8961 (2022).
125. Sun, F.-S. *et al.* Organic carbon preservation in wetlands: Iron oxide protection vs. thermodynamic limitation. *Water Research* **241**, 120133. ISSN: 0043-1354 (Aug. 2023).
126. Thompson, A., Chadwick, O. A., Boman, S. & Chorover, J. Colloid Mobilization During Soil Iron Redox Oscillations. *Environmental Science & Technology* **40**. 5743–5749. ISSN: 0013-936X (Sept. 2006).
127. Thompson, A., Rancourt, D. G., Chadwick, O. A. & Chorover, J. Iron solid-phase differentiation along a redox gradient in basaltic soils. *Geochimica et Cosmochimica Acta* **75**, 119–133. ISSN: 0016-7037 (Jan. 2011).
128. Tiedje, J. M., Sexstone, A. J., Parkin, T. B. & Revsbech, N. P. Anaerobic processes in soil. en. *Plant and Soil* **76**, 197–212. ISSN: 0032-079X, 1573-5036 (Feb. 1984).
129. Vanmarcke, E. *Random fields, analysis and synthesis* English. ISBN: 978-0-262-22026-2 (Cambridge, Mass: MIT Press, 1983).
130. Wagener, T. & Kollat, J. Numerical and visual evaluation of hydrological and environmental models using the Monte Carlo analysis toolbox. *Environmental Modelling & Software* **22**, 1021–1033. ISSN: 1364-8152 (July 2007).
131. Waksman, S. A. What Is Humus?1. *Proceedings of the National Academy of Sciences* **11**. 463–468 (Aug. 1925).
132. Waksman, S. A. *Humus: Origin, Chemical Composition, and Importance in Nature* (The Williams & Wilkins Company, Baltimore, Jan. 1936).
133. Wang, Y.-P. *et al.* Toward a Global Model for Soil Inorganic Phosphorus Dynamics: Dependence of Exchange Kinetics and Soil Bioavailability on Soil Physicochemical Properties. en. *Global Biogeochemical Cycles* **36**. e2021GB007061. ISSN: 1944-9224 (Mar. 2022).

134. Wang, Y., Wang, H., He, J.-S. & Feng, X. Iron-mediated soil carbon response to water-table decline in an alpine wetland. en. *Nature Communications* **8**. 15972. ISSN: 2041-1723 (June 2017).
135. Wang, Y. *et al.* Evaluating wetland soil carbon stability related to iron transformation during redox oscillations. *Geoderma* **428**, 116222. ISSN: 0016-7061 (Dec. 2022).
136. Weiss, J. V., Emerson, D. & Megonigal, J. P. Geochemical control of microbial Fe(III) reduction potential in wetlands: comparison of the rhizosphere to non-rhizosphere soil. *FEMS Microbiology Ecology* **48**, 89–100. ISSN: 0168-6496 (Apr. 2004).
137. Wieder, W. R. *et al.* Carbon cycle confidence and uncertainty: Exploring variation among soil biogeochemical models. en. *Global Change Biology* **24**. 1563–1579. ISSN: 1365-2486 (2018).
138. Woolf, D. & Lehmann, J. Microbial models with minimal mineral protection can explain long-term soil organic carbon persistence. en. *Scientific Reports* **9**. 6522. ISSN: 2045-2322 (Apr. 2019).
139. Wu, S., Konhauser, K. O., Chen, B. & Huang, L. “Reactive Mineral Sink” drives soil organic matter dynamics and stabilization. en. *npj Materials Sustainability* **1**. 1–12. ISSN: 2948-1775 (Nov. 2023).
140. Ye, C., Huang, W., Hall, S. J. & Hu, S. Association of Organic Carbon With Reactive Iron Oxides Driven by Soil pH at the Global Scale. en. *Global Biogeochemical Cycles* **36**. e2021GB007128. ISSN: 1944-9224 (2022).
141. Yu, G. *et al.* Mineral Availability as a Key Regulator of Soil Carbon Storage. *Environmental Science & Technology* **51**. 4960–4969. ISSN: 0013-936X (May 2017).
142. Zakem, E. J., Cael, B. B. & Levine, N. M. A unified theory for organic matter accumulation. *Proceedings of the National Academy of Sciences* **118**. e2016896118 (Feb. 2021).
143. Zhao, H. *et al.* Soil organic carbon stabilization and associated mineral protection in typical coastal wetlands under different hydrologic conditions. *Frontiers in Marine Science* **9**. ISSN: 2296-7745 (2022).
144. Zhao, Q. *et al.* Iron-bound organic carbon in forest soils: quantification and characterization. English. *Biogeosciences* **13**. 4777–4788. ISSN: 1726-4170 (Aug. 2016).
145. Zhao, Q. *et al.* Coupled dynamics of iron and iron-bound organic carbon in forest soils during anaerobic reduction. *Chemical Geology. Adsorption of metals by geomedial III: Fundamentals and implications of metal adsorption* **464**, 118–126. ISSN: 0009-2541 (Aug. 2017).
146. Zheng, G., Chen, J. & Li, W. Impacts of CO₂ elevation on the physiology and seed quality of soybean. *Plant Diversity* **42**, 44–51. ISSN: 2096-2703 (Oct. 2019).
147. Zhu, E. *et al.* Leaching of organic carbon from grassland soils under anaerobiosis. *Soil Biology and Biochemistry* **141**, 107684. ISSN: 0038-0717 (Feb. 2020).